Collisional Delta-f Scheme with Evolving Background for Transport Time Scale Simulations

S. Brunner*, E. Valeo, and J. A. Krommes

Princeton Plasma Physics Laboratory, P.O. Box 451, Princeton, New Jersey 08543–0451

Abstract

The δf approach is extended for simulating the transport time-scale evolution of near-Maxwellian distributions in collisional plasmas. This involves simultaneously advancing weighted marker particles for representing the intrinsically kinetic component δf, and fluid equations for the parameters of the shifted Maxwellian background f_{SM}. The issue of increasing numerical noise in a collisional δf algorithm, due to marker particle weight spreading, is addressed in detail, and a solution to this problem is proposed. To obtain higher resolution in critical regions of phase space, a practical procedure for implementing sources and sinks of marker particles is developed. As a proof of principal, this set of methods are applied for computing electrical Spitzer conductivity as well as collisional absorption in a homogeneous plasma.

52.65.Ff, 52.65.Pp, 52.40.Nk

*E-mail: sbrunner@pppl.gov

I. INTRODUCTION

The δf algorithm[1–3] has been widely applied in magnetic fusion, mainly for studying anomalous transport induced by microturbulence.[4] Due to the limits of present day computer power, these complex five-dimensional gyrokinetic simulations are still carried out over real-time periods short compared to confinement times. Therefore, only particle and energy fluxes are computed, but not the actual relaxation of global profiles and particle distributions. For this reason, the only component of a given species distribution that has been evolved in time when applying the δf approach in this context was the deviation (i.e. δf) from a fixed equilibrium-like background $\overline{f}$.

In view of longer real-time simulations, but also with the interest of applying the δf method to a broader range of problems, we investigate in this paper the issues involved in extending this procedure to transport time scale simulations. If the advantages of the δf method are to be preserved over such times, during which the bulk of the particle distributions are evolving, the background component $\overline{f}$ must now also be advanced, together with the deviation δf, so that the ratio $\delta f/\overline{f}$ remains small[1,5,6] at all times. A similar procedure had been proposed in the past for collisionless plasmas,[7] but to our knowledge its implementation has not been pursued.

The right choice for the shape and evolution of the background $\overline{f}$, so that it remains a good approximation of the full distribution $f = \overline{f} + \delta f$ at all times, is a subtle point in general. In this respect, restricting the study to collisional systems is helpful, as the choice of a local shifted Maxwellian distribution f_{SM} for $\overline{f}$ appears naturally. We shall therefore be considering collisional plasmas in the following. The parameters (density, average velocity and thermal velocity) of the background f_{SM} are then evolved according to numerically "cheap" fluid equations, with closure calculated correctly from the intrinsically kinetic part δf. The simultaneous evolution of δf and the fluid equations thus defines a self-consistent hybrid fluid-kinetic procedure.

On the other hand, the implementation of collisions in a δf algorithm is an issue in itself.[8–11] In particular, as discussed by Chen and White,[11] the practical implementation of collisions in a δf algorithm requires the marker particle weights to be interpreted statistically: As the result of collisions, particles having carried out different random trajectories can end up at a same point $(\boldsymbol{x}, \boldsymbol{v})$ in phase space with different weights. We shall refer to this effect as the spreading Δw of marker particle weights. The actual weight field $W(\boldsymbol{x}, \boldsymbol{v}) = \delta f(\boldsymbol{x}, \boldsymbol{v})/\overline{f}(\boldsymbol{x}, \boldsymbol{v})$ at a given point $(\boldsymbol{x}, \boldsymbol{v})$ in phase space must then be interpreted as the average over all marker particle weights in the vicinity of $(\boldsymbol{x}, \boldsymbol{v})$.

Although Chen and White established the formalism for a rigorous derivation of the δf scheme in collisional systems,[11] by working in an extended marker particle phase space $(\boldsymbol{x}, \boldsymbol{v}, w)$, position, velocity and weight, they did not, however, point out that Δw keeps on increasing. Over many collision times, this would ultimately lead to the breakdown of the δf approach. Indeed, the spreading Δw in time can be viewed as an additional growing dimension of the system, requiring always more particles to resolve.

Hence, in deriving a practical collisional δf algorithm for transport time scale simulations one must deal with two essential problems: the spreading of weights due to collisions and the evolution of the background. The first point will be addressed in Sec. II, where we shall start by reviewing the origin of marker particle weight spreading and its evolution in the case of a distribution relaxing through self-collisions. A possible solution for reducing Δw will be proposed. The derivation of appropriate fluid equations for the evolution of the background parameters will be shown in Sec. III in the case of two illustrations for homogeneous plasmas: 1) D.C. electrical conductivity, and 2) collisional absorption of a high frequency electrical field. Conclusions are drawn in Sec. IV. Finally, some technical details relative to a reduced model for the self-collision operator, proposed by Lin et al.,[10] are given in Appendix A, and a practical method for adding sources and sinks of markers to obtain better resolution in critical regions of phase space is presented in Appendix B.

II. SPREADING OF MARKER PARTICLE WEIGHTS IN COLLISIONAL SYSTEMS – CONSIDERING THE RELAXATION OF A DISTRIBUTION THROUGH SELF-COLLISIONS

A. Starting Equations

For studying particle weight spreading, let us reduce the Fokker–Planck equation to the terms that account for this effect: collisions. We therefore consider in this section the relaxation in velocity space of a distribution $f(\boldsymbol{v};t)$ of particles through self-collisions:

$$\frac{\partial f}{\partial t} = -C[f,f], \tag{1}$$

where $C[f_2,f_1]$, representing collisions of distribution f_1 on distribution f_2, is given here by the Landau operator:

$$C[f_2,f_1] = \Gamma \frac{\partial}{\partial \boldsymbol{v}} \cdot \int d\boldsymbol{v}\,' \mathsf{U}(\boldsymbol{v}-\boldsymbol{v}\,')\left[\frac{\partial}{\partial \boldsymbol{v}\,'} - \frac{\partial}{\partial \boldsymbol{v}}\right] f_2(\boldsymbol{v}\,') f_1(\boldsymbol{v}), \tag{2}$$

with $\Gamma = \overline{N} q^4 \ln\Lambda / 8\pi\epsilon_0^2 m^2$ and $\mathsf{U}(\boldsymbol{u}) = (u^2\mathbf{1} - \boldsymbol{u}\boldsymbol{u})/u^3$. For the following discussion, it is useful to cast the Landau operator in the drift-diffusion form:

$$C[f_2,f_1] = \frac{\partial}{\partial \boldsymbol{v}} \cdot \left[\boldsymbol{R}(\boldsymbol{v}) f_1(\boldsymbol{v}) - \frac{\partial}{\partial \boldsymbol{v}} \cdot \mathsf{D}(\boldsymbol{v}) f_1(\boldsymbol{v})\right],$$

where drag and the diffusion tensor are given by

$$\boldsymbol{R}(\boldsymbol{v}) = -2\,\Gamma \int d\boldsymbol{v}\,' \frac{\partial}{\partial \boldsymbol{v}\,'} \cdot \mathsf{U}(\boldsymbol{v}-\boldsymbol{v}\,') f_2(\boldsymbol{v}\,'),$$
$$\mathsf{D}(\boldsymbol{v}) = \Gamma \int d\boldsymbol{v}\,' \mathsf{U}(\boldsymbol{v}-\boldsymbol{v}\,') f_2(\boldsymbol{v}\,').$$

Let us now apply the δf method for solving Eq. (1). For this purpose, the full distribution $f(\boldsymbol{v};t)$ is decomposed here into a stationary Maxwellian background $f_{\mathrm{M}}(v)$ and the remainder $\delta f(\boldsymbol{v};t)$:

$$f(\boldsymbol{v};t) = f_{\mathrm{M}}(v) + \delta f(\boldsymbol{v};t),$$
$$f_{\mathrm{M}}(v) = \frac{1}{(2\pi v_{\mathrm{th}}^2)^{3/2}} \exp\left(-\frac{v^2}{2v_{\mathrm{th}}^2}\right).$$

Inserting this decomposition in the bilinear collision operator leads to

$$C[f,f] = C[f_{\rm M}, f_{\rm M}] + C[\delta f, \delta f] + C[f_{\rm M}, \delta f] + C[\delta f, f_{\rm M}].$$

The full collision operator annihilates the Maxwellian distribution, so that the first term on the right-hand side is zero. Furthermore, assuming only small deviations from the background, the second term, which is nonlinear in δf, will be neglected here. The evolution of δf is now reduced to the linearized collision operator:

$$\frac{\partial \delta f}{\partial t} = -\left\{C[f_{\rm M}, \delta f] + C[\delta f, f_{\rm M}]\right\} \equiv -\widehat{C}\delta f. \tag{3}$$

This equation is appropriate, for instance, for describing the relaxation of a low-density beam off of a Maxwellian background. The relaxed states of Eq. (3), i.e., the functions annihilated by $\widehat{C}$, are of the form

$$\lim_{t\to\infty} \delta f(\boldsymbol{v};t) = \left[c_0 + \boldsymbol{c}_1 \boldsymbol{\cdot} \boldsymbol{v}/v_{\rm th} + c_2 (v/v_{\rm th})^2\right] f_{\rm M}(v), \tag{4}$$

representing linearized perturbations in density, average velocity and temperature of the background $f_{\rm M}$. The constants c_0, $\boldsymbol{c}_1$, and c_2 are determined by the initial state through conservation of particles, momentum, and energy.

Let us also define the operator

$$\frac{D}{Dt} \doteq \frac{\partial}{\partial t} + C[f_{\rm M},\ ], \tag{5}$$

so that the equation for δf can be written

$$\frac{D}{Dt}\delta f = -C[\delta f, f_{\rm M}]. \tag{6}$$

B. Attempting to Apply the Standard δf Procedure

Carrying on with the standard δf procedure originally developed for collisionless systems, δf is represented as the product of the marker particle distribution $g(\boldsymbol{v};t)$ and the weight field $W(\boldsymbol{v};t)$:

$$\delta f(\boldsymbol{v};t) = g(\boldsymbol{v};t)W(\boldsymbol{v};t). \tag{7}$$

For the evolution of the marker particle distribution, it is practical to choose

$$\frac{D}{Dt}g = 0, \tag{8}$$

which represents the scattering of test particles the fixed Maxwellian background. Equation (8) is resolved by representing g with a finite number n_p of marker particles:

$$g(\boldsymbol{v};t) \simeq \widehat{g}(\boldsymbol{v};t) = \sum_{i=1}^{n_p} \delta(\boldsymbol{v} - \boldsymbol{v}_i(t)).$$

The trajectories $\boldsymbol{v}_i(t)$ are computed by applying a well-established Monte-Carlo method,[12] which correctly reproduces the scattering off of the Maxwellian background as described by the Landau operator. Over each time step Δt, particles undergo random velocity increments $\Delta\boldsymbol{v}$ such that

$$\frac{\langle \Delta\boldsymbol{v}\,\rangle}{\Delta t} = \boldsymbol{R}(\boldsymbol{v}) = -\overline{\nu}\, v_{\text{th}} H \frac{\boldsymbol{v}}{v_{\text{th}}}, \tag{9}$$

$$\frac{\langle \Delta\boldsymbol{v}\,\Delta\boldsymbol{v}\,\rangle}{\Delta t} = 2\mathsf{D}(\boldsymbol{v}) = \frac{\overline{\nu}\, v_{\text{th}}^2}{2}\left[K\left(1 - \frac{\boldsymbol{v}\,\boldsymbol{v}}{v^2}\right) + 2H\frac{\boldsymbol{v}\,\boldsymbol{v}}{v^2}\right], \tag{10}$$

with $\overline{\nu} = \overline{N} q^4 \ln\Lambda / 2\pi\epsilon_0^2 m^2 v_{\text{th}}^3$ being the thermal self-collision frequency. In (9) and (10) the drag and diffusion tensor have been computed for the Maxwellian background and expressed in terms of the Rosenbluth potentials $H = H(v/v_{\text{th}})$ and $K = K(v/v_{\text{th}})$:[13]

$$H(x) = \frac{1}{x^3}\Big[\text{erf}(x/\sqrt{2}) - \sqrt{\frac{2}{\pi}}x\, e^{-x^2/2}\Big], \tag{11}$$

$$K(x) = \frac{1}{x^3}\Big[(x^2-1)\text{erf}(x/\sqrt{2}) + \sqrt{\frac{2}{\pi}}x\, e^{-x^2/2}\Big], \tag{12}$$

using the definition $\text{erf}(x) = (2/\sqrt{\pi})\int_0^x dt\, \exp(-t^2)$ for the error function. In an orthogonal coordinate system (x', y', z'), such that the direction z' is parallel to the incoming velocity $\boldsymbol{v}$ of a given marker particle, the random velocity increment after a time Δt ($\overline{\nu}\Delta t \ll 1$) can thus be written

$$\Delta v_{x'} = v_{\text{th}}\sqrt{(\overline{\nu}\Delta t/2)K(v/v_{\text{th}})}R_{x'}, \tag{13}$$

$$\Delta v_{y'} = v_{\text{th}}\sqrt{(\overline{\nu}\Delta t/2)K(v/v_{\text{th}})}R_{y'}, \tag{14}$$

$$\Delta v_{x'} = -\overline{\nu}\Delta t\, H(v/v_{\text{th}})v + v_{\text{th}}\sqrt{\overline{\nu}\Delta t H(v/v_{\text{th}})}R_{z'}, \tag{15}$$

where $R_{x'}$, $R_{y'}$, and $R_{z'}$ are independent random numbers with zero mean and unit root mean square width.

To complete the structure for the δf procedure, an equation is still required for the marker particle weight w_i. We will start by considering the definition for w_i used in collisionless systems, that is, the value of the weight field at the position of the particle:

$$w_i(t) = W(\boldsymbol{v}_i(t); t). \tag{16}$$

In the following, we will make use of the relation between the operator d/dt:

$$\frac{d}{dt} \doteq \frac{\partial}{\partial t} + (\boldsymbol{R} + \boldsymbol{a}_c)\boldsymbol{\cdot}\frac{\partial}{\partial \boldsymbol{v}},$$

representing the total time derivative along the stochastic trajectory of a given particle, and the operator D/Dt defined by (5):

$$\frac{d}{dt} = \frac{D}{Dt} - (\frac{\partial}{\partial \boldsymbol{v}}\boldsymbol{\cdot}\boldsymbol{R}) + \boldsymbol{a}_c\boldsymbol{\cdot}\frac{\partial}{\partial \boldsymbol{v}} + \frac{\partial^2}{\partial \boldsymbol{v}\partial \boldsymbol{v}} : \mathsf{D}, \tag{17}$$

where $\boldsymbol{a}_c$ stands for the random acceleration relative to collisions with the background distribution. The second term on the right-hand side of relation (17) is related to the compressibility of the velocity space flux due to drag, and the two last terms are related to diffusion. Note that d/dt is a first order differential operator, while D/Dt, in general, is second order. Making use of the chain rule for the first-order differential operator d/dt, relation (17), as well as definitions (16) and (7), one can derive

$$\begin{aligned}\frac{d}{dt}w_i(t) &= \frac{d}{dt}W(\boldsymbol{v}_i(t); t) = \frac{d}{dt}\frac{\delta f}{g} = \frac{1}{g}\frac{d\delta f}{dt} - \frac{\delta f}{g^2}\frac{dg}{dt} \\ &= \frac{1}{g}\left[\frac{D}{Dt}\delta f - (\frac{\partial}{\partial \boldsymbol{v}}\boldsymbol{\cdot}\boldsymbol{R})\delta f + \boldsymbol{a}_c\boldsymbol{\cdot}\frac{\partial \delta f}{\partial \boldsymbol{v}} + \frac{\partial^2}{\partial \boldsymbol{v}\partial \boldsymbol{v}} : (\mathsf{D}\delta f)\right] \\ &\quad -\frac{\delta f}{g^2}\left[\frac{D}{Dt}g - (\frac{\partial}{\partial \boldsymbol{v}}\boldsymbol{\cdot}\boldsymbol{R})g + \boldsymbol{a}_c\boldsymbol{\cdot}\frac{\partial g}{\partial \boldsymbol{v}} + \frac{\partial^2}{\partial \boldsymbol{v}\partial \boldsymbol{v}} : (\mathsf{D}g)\right].\end{aligned} \tag{18}$$

Inserting the evolution equations (6), and (8), one then obtains

$$\frac{d}{dt}w_i(t) = -\frac{1}{g}C[\delta f, f_{\mathrm{M}}] + \frac{1}{g}\left[\boldsymbol{a}_c\boldsymbol{\cdot}\left(\frac{\partial \delta f}{\partial \boldsymbol{v}} - w_i\frac{\partial g}{\partial \boldsymbol{v}}\right) + \frac{\partial^2}{\partial \boldsymbol{v}\partial \boldsymbol{v}} : (\mathsf{D}\delta f) - w_i\frac{\partial^2}{\partial \boldsymbol{v}\partial \boldsymbol{v}} : (\mathsf{D}g)\right], \tag{19}$$

where all fields on the right-hand side are evaluated at the particle position $\boldsymbol{v} = \boldsymbol{v}_i(t)$.

C. The Practical Weight Equation in a Collisional System and the Problem of Marker Particle Weight Spreading

In practice,[8–11] only the first term on the right-hand side of Eq.(19) is kept, so that the equation that is actually implemented for numerical simulations reads

$$\frac{d}{dt}w_i(t) = -\frac{1}{g}C[\delta f, f_{\mathrm{M}}]. \tag{20}$$

This is the equation that one would formally derive from (18) by not considering the difference, pointed out in (17), between the operators d/dt and D/Dt. Note that the term in (17) related to the compressibility of drag actually cancels out in deriving (19), so that all terms omitted in (20) compared to (19) are related to diffusion. The practical reason for omitting these contributions is that they require evaluating partial derivatives in velocity space of the fields g and δf, at each time step and at each particle position. Besides being costly numerically, such an operation is demanding statistically and therefore avoided.

The effect of the terms that have been discarded in (20) was to ensure that two particles end up with the same value of their weight in case they meet at the same point in phase space after having undergone different stochastic trajectories, in agreement with the initial definition (16). Thus, removing these terms leads to a spreading of particle weights in phase space, that is, different particles end up at the same point with different values of w_i, in contradiction with (16).

The difference between a collisional and collisionless δf simulation is shown schematically in figure 1. In the absence of collisions (Fig. 1a), although there may be a global increase of weight variance (also called entropy),[14–16] related e.g. to always finer growing structure in δf, there is only one possible marker weight value at each time and position in phase space. In other words, the local weight spread Δw is zero. However, in the presence of collisions (Fig.1.b), a spread Δw of marker weights appears at each point in phase space, which, in general, keeps on increasing over time.

D. The Extended Phase Space Formalism together with the Two-Weight Scheme

Evidently, if the system of equations (13)–(15) and (20) is correct in any sense, the meaning of marker weights has to be reconsidered. Chen and White[11] have shown that the weight field W at a given point in phase space must be interpreted as the average over all particle weights at that point, and have proven that the system of equations for the marker particles, including (20) for the weights evolution, is exact in this sense in the limit of large particle number. For this purpose, they introduce the marker particle distribution $F(\boldsymbol{v}, w; t)$ in the extended phase space $(\boldsymbol{v}, w)$.

In fact, let us extend Chen and White's formalism to include the generalized weighting scheme proposed by Hu and Krommes[6] for avoiding the evaluation of the distribution g appearing in (20). This involves defining a second weight field P:

$$f_{\mathrm{M}}(v) = P(\boldsymbol{v}; t) g(\boldsymbol{v}; t), \tag{21}$$

and again starting by defining the second marker particle weights by

$$p_i(t) = P(\boldsymbol{v}_i(t); t). \tag{22}$$

In the same way as the evolution equation for $w_i(t)$ was derived, one obtains for $p_i(t)$

$$\frac{d}{dt} p_i(t) = 0, \tag{23}$$

having used

$$\frac{D}{Dt} f_{\mathrm{M}}(v) = 0 \tag{24}$$

and again discarded terms related to diffusion, which requires the same statistical reinterpretation of the weights p_i as of weights w_i. In this two-weight scheme, (20) now reads

$$\frac{d}{dt} w_i(t) = -p_i(t) \frac{C[\delta f, f_{\mathrm{M}}]}{f_{\mathrm{M}}}. \tag{25}$$

Hence, to prove that the system of equations (13)–(15), (23) and (25) is correct in the average sense described above, let us define the marker particle distribution $F(\boldsymbol{v}, w, p; t)$

in the extended phase space $(\boldsymbol{v}, w, p)$. According to the equivalence between Langevian equations and the Fokker–Planck equation, the kinetic equation for F is given by

$$\frac{\partial F}{\partial t} + C[f_{\mathrm{M}}, F] + \frac{\partial}{\partial w}\left(-p\frac{C[\delta f, f_{\mathrm{M}}]}{f_{\mathrm{M}}}F\right) = 0, \tag{26}$$

and the initial condition, with zero spreading along w and p, by

$$F(\boldsymbol{v}, w, p; t=0) = g_0(\boldsymbol{v})\,\delta(w - W_0(\boldsymbol{v}))\,\delta(p - P_0(\boldsymbol{v})), \tag{27}$$

with $W_0(\boldsymbol{v}) = \delta f(\boldsymbol{v}; t=0)/g_0(\boldsymbol{v})$ and $P_0(\boldsymbol{v}) = f_{\mathrm{M}}(v)/g_0(\boldsymbol{v})$.

By taking the moments $\int dw\,dp$, $\int p\,dw\,dp$, $\int w\,dw\,dp$ of (26)–(27) and interpreting:

$$g(\boldsymbol{v}; t) = \int dw\,dp\,F(\boldsymbol{v}, w, p; t), \tag{28}$$

$$f_{\mathrm{M}}(v) = \int dw\,dp\,p\,F(\boldsymbol{v}, w, p; t), \tag{29}$$

$$\delta f(\boldsymbol{v}; t) = \int dw\,dp\,w\,F(\boldsymbol{v}, w, p; t), \tag{30}$$

one can easily show that one recovers the equations (8), (24) and (6) for the evolution of these three fields with corresponding initial conditions, which proves that the system of equations is correct.

Note that for F represented with n_p marker particles and approximated by the coarse grained function $\widehat{F}$,

$$F(\boldsymbol{v}, w, p; t) \simeq \widehat{F}(\boldsymbol{v}, w, p; t) = \sum_{i=1}^{n_p} \delta(\boldsymbol{v} - \boldsymbol{v}_i(t))\,\delta(p - p_i(t))\,\delta(w - w_i(t)), \tag{31}$$

one still recovers, using (28) and (30), the usual relations as for the collisionless δf scheme:

$$g(\boldsymbol{v}; t) \simeq \widehat{g}(\boldsymbol{v}; t) = \sum_{i=1}^{n_p} \delta(\boldsymbol{v} - \boldsymbol{v}_i(t)),$$

$$\delta f(\boldsymbol{v}; t) \simeq \delta\widehat{f}(\boldsymbol{v}; t) = \sum_{i=1}^{n_p} w_i(t)\,\delta(\boldsymbol{v} - \boldsymbol{v}_i(t)).$$

Also, inserting (28)–(30) in (7) and (21) gives

$$W(\boldsymbol{v}; t) = \int dw\,dp\,w\,F(\boldsymbol{v}, w, p; t) \Big/ \int dw\,dp\,F(\boldsymbol{v}, w, p; t),$$

$$P(\boldsymbol{v}; t) = \int dw\,dp\,p\,F(\boldsymbol{v}, w, p; t) \Big/ \int dw\,dp\,F(\boldsymbol{v}, w, p; t),$$

clearly showing that the weight fields W and P are given by the average over all particle weights w_i and p_i at a given point $\boldsymbol{v}$.

E. Evolution of Weight Spreading and Entropy

What we shall now discuss in more detail is the evolution of the marker particle weight spread Δw:

$$
\begin{aligned}
(\Delta w_{(\boldsymbol{v};t)})^2 = \langle w^2 \rangle_{(\boldsymbol{v};t)} - \langle w \rangle_{(\boldsymbol{v};t)}{}^2 &= \frac{\int F\, w^2 dw\, dp}{\int F\, dw\, dp} - \left(\frac{\int F\, w\, dw\, dp}{\int F\, dw\, dp} \right)^2 \\
&= \frac{1}{g} \int F\, w^2 dw\, dp - W^2.
\end{aligned}
\tag{32}
$$

We shall also make use of the average weight spread defined as the integral over the total phase space of the appropriately weighted local spread:

$$
(\Delta w_{\rm tot})^2 = \frac{\int (\Delta w_{(\boldsymbol{v};t)})^2 F\, dw\, dp\, d\boldsymbol{v}}{\int F dw\, dp\, d\boldsymbol{v}} = \frac{1}{n_p} \int g\, (\Delta w_{(\boldsymbol{v};t)})^2 d\boldsymbol{v}. \tag{33}
$$

According to (32) and (33), the total weight spread $\Delta w_{\rm tot}$ is related to the entropy-like quantity

$$
\mathcal{S}_w(t) = \frac{1}{2} \int w^2\, F\, dw\, dp\, d\boldsymbol{v} \tag{34}
$$

through

$$
\mathcal{S}_w = \mathcal{F} + \frac{n_p}{2} (\Delta w_{\rm tot})^2, \tag{35}
$$

where $\mathcal{F}(t) = (1/2) \int g\, W^2 d\boldsymbol{v}$ is the definition of entropy in a collisionless system.[14,15]

The definitions for $\mathcal{S}_w$ and $\mathcal{F}$ naturally coincide in the absence of weight spreading. However, using (31), note that it is $\mathcal{S}_w$, and not $\mathcal{F}$, that can in all cases be written

$$
\mathcal{S}_w(t) \simeq \frac{1}{2} \sum_{i=1}^{n_p} w_i^2(t). \tag{36}
$$

Taking the moment $(1/2) \int w^2\, dw\, dp\, d\boldsymbol{v}$ of (26) provides an equation for the evolution of $\mathcal{S}_w(t)$:

$$
\frac{d}{dt} \mathcal{S}_w(t) = - \int \frac{C[\delta f, f_{\rm M}]}{f_{\rm M}} w\, p\, F dw\, dp\, d\boldsymbol{v},
$$

having used the conservation of particles by the collision operator. With the idea of clearly pointing out the marker particle weight spreading, let us carry on with the analytical derivation and consider the entropy evolution asymptotically in time, when both δf and g have relaxed towards stationary states. According to (8), g always relaxes to $n_p f_{\rm M}$, so that on average one finally has $\langle p_i \rangle = P = 1/n_p$. By assuming that already initially $g(\boldsymbol{v}; t=0) \doteq g_0(\boldsymbol{v}) = n_p f_{\rm M}(\boldsymbol{v})$, one has $p_i(t) = 1/n_p = \text{const}$ for all particles. The equation for $\mathcal{S}_w$ can then be written

$$\begin{aligned}\frac{d}{dt}\mathcal{S}_w(t) &= -\frac{1}{n_p}\int \frac{\delta f}{f_{\rm M}} C[\delta f, f_{\rm M}]\, d\boldsymbol{v} \\ &= \frac{\Gamma}{n_p}\int f_{\rm M}(\boldsymbol{v}) f_{\rm M}(\boldsymbol{v}')\frac{\partial}{\partial \boldsymbol{v}}\left(\frac{\delta f(\boldsymbol{v})}{f_{\rm M}(\boldsymbol{v})}\right)\cdot \mathsf{U}(\boldsymbol{v}-\boldsymbol{v}')\cdot\frac{\partial}{\partial \boldsymbol{v}'}\left(\frac{\delta f(\boldsymbol{v}')}{f_{\rm M}(\boldsymbol{v}')}\right) d\boldsymbol{v}\, d\boldsymbol{v}', \end{aligned} \tag{37}$$

having applied the relation

$$\int a(\boldsymbol{v}) C[b f_{\rm M}, f_{\rm M}] d\boldsymbol{v} = -\Gamma \int f_{\rm M}(\boldsymbol{v}) \frac{\partial a(\boldsymbol{v})}{\partial \boldsymbol{v}}\cdot \mathsf{U}(\boldsymbol{v}-\boldsymbol{v}')\cdot \frac{\partial b(\boldsymbol{v}')}{\partial \boldsymbol{v}'} f_{\rm M}(\boldsymbol{v}') d\boldsymbol{v}\, d\boldsymbol{v}',$$

for $a = b = \delta f / f_{\rm M}$. Inserting the general stationary form (4) for δf in (37) gives

$$\begin{aligned}\frac{d}{dt}\mathcal{S}_w(t) &= \frac{\Gamma}{n_p}\int f_{\rm M}(\boldsymbol{v}) f_{\rm M}(\boldsymbol{v}')(\boldsymbol{c_1} + 2c_2\boldsymbol{v})\cdot \mathsf{U}(\boldsymbol{v}-\boldsymbol{v}')\cdot(\boldsymbol{c_1}+2c_2\boldsymbol{v}')d\boldsymbol{v}\, d\boldsymbol{v}' \\ &= \frac{\Gamma}{n_p}\int f_{\rm M}(\boldsymbol{v}) f_{\rm M}(\boldsymbol{v}')\frac{|\boldsymbol{c_1}+2c_2\boldsymbol{v}|^2}{|\boldsymbol{v}-\boldsymbol{v}'|}\left[1-\left(\frac{\boldsymbol{v}-\boldsymbol{v}'}{|\boldsymbol{v}-\boldsymbol{v}'|}\cdot\frac{\boldsymbol{c_1}+2c_2\boldsymbol{v}}{|\boldsymbol{c_1}+2c_2\boldsymbol{v}|}\right)^2\right] d\boldsymbol{v}\, d\boldsymbol{v}', \end{aligned} \tag{38}$$

having made use of $\mathsf{U}\cdot(\boldsymbol{v}-\boldsymbol{v}') = 0$. The right-hand side of (38) is strictly positive, except in the trivial case where $\delta f = c_0 f_{\rm M}$ ($c_1, c_2 = 0$), so that $\mathcal{S}_w$ keeps on increasing linearly in time. According to (35), together with the fact that $\mathcal{F}$ is constant once δf and g are stationary, this can only be explained by a spreading of marker particle weights, which scales as $\Delta w \sim \sqrt{t}$.

Equivalent quantities to (32), (33), and (34) can be defined for the second weight p. For the particular system considered here, where $p_i(t) = \text{const}$ [Eq. (23)], one has $\mathcal{S}_p = (1/2)\int p^2\, F\, dw\, dp\, d\boldsymbol{v} = \text{const}$. Thus, from the relation equivalent to (35),

$$\mathcal{S}_p = \frac{1}{2}\int g\, P^2\, d\boldsymbol{v} + \frac{n_p}{2}(\Delta p_{\rm tot})^2,$$

one can conclude that the spreading of weights p does not increase in this case once g has relaxed to its stationary state $g(t\to\infty) = n_p f_{\rm M}$.

F. Increasing Numerical Noise Due to Weight Spreading

In general, when carrying out a δf simulation with collisions, both Δw and Δp keep on growing throughout the run. This would require an ever-increasing number n_p of marker particles to ensure a given accuracy of the computation. Indeed, if for example one intends to evaluate $\delta f(\boldsymbol{z})$ at a given point $\boldsymbol{z} = (\boldsymbol{x}, \boldsymbol{v})$ in phase space, one applies the estimator

$$E \doteq \frac{1}{\Delta V_{\boldsymbol{z}}} \sum_{i=1}^{n_b} w_i \simeq \delta f(\boldsymbol{z}),$$

where n_b are the number of particles in a small phase-space bin $\Delta V_{\boldsymbol{z}}$ centered at $\boldsymbol{z}$ (see Fig. 1b). Assuming for simplification that n_b and all weights w_i are uncorrelated, and that $W(\boldsymbol{z})$ and $\Delta w_{\boldsymbol{z}}$ can be considered constant over the volume $\Delta V_{\boldsymbol{z}}$, one can evaluate the mean and variance of E:

$$\begin{aligned}
\langle E \rangle &= \frac{1}{\Delta V_{\boldsymbol{z}}} \langle n_b \rangle W(\boldsymbol{z}), \\
\langle E^2 \rangle &= \frac{1}{(\Delta V_{\boldsymbol{z}})^2} \langle \sum_{i=1}^{n_b} w_i^2 + 2 \sum_{i<j=1}^{n_b} w_i \, w_j \rangle = \frac{1}{(\Delta V_{\boldsymbol{z}})^2} \left[\langle n_b \rangle \langle w_i^2 \rangle + 2 \frac{\langle n_b(n_b - 1) \rangle}{2} \langle w_i \rangle \langle w_j \rangle \right] \\
&= \frac{1}{(\Delta V_{\boldsymbol{z}})^2} \left[\langle n_b \rangle (\Delta w_{\boldsymbol{z}})^2 + \langle n_b^2 \rangle W(\boldsymbol{z})^2 \right], \\
(\Delta E)^2 = \langle E^2 \rangle - \langle E \rangle^2 &= \frac{1}{(\Delta V_{\boldsymbol{z}})^2} \left[(\Delta n_b)^2 W(\boldsymbol{z})^2 + \langle n_b \rangle (\Delta w_{\boldsymbol{z}})^2 \right],
\end{aligned}$$

so that the relative deviation is given by

$$\frac{\Delta E}{\langle E \rangle} = \sqrt{\frac{(\Delta n_b)^2}{\langle n_b \rangle^2} + \frac{(\Delta w_{\boldsymbol{z}})^2}{\langle n_b \rangle W(\boldsymbol{z})^2}} = \sqrt{\frac{1 - p_{\text{in}}}{n_p \, p_{\text{in}}} + \frac{(\Delta w_{\boldsymbol{z}})^2}{n_p \, p_{\text{in}} W(\boldsymbol{z})^2}}, \tag{39}$$

having used $(\Delta n_b)^2 = n_p \, p_{\text{in}}(1 - p_{\text{in}})$ and $\langle n_b \rangle = n_p \, p_{\text{in}}$, where $p_{\text{in}} = \Delta V_{\boldsymbol{z}} \, g(\boldsymbol{z})/n_p$ is the probability for a particle to fall in the bin $\Delta V_{\boldsymbol{z}}$. The first contribution under the square root on the right-hand side of Eq.(39) is related to the fluctuating number n_b of particles in the bin and corresponds to the sampling noise already present in collisionless δf simulations.[6] The second term is related to Δw, which thus only appears in collisional simulations. To maintain the statistical noise below a certain level, the total number n_p of marker particles would therefore eventually have to increase as

$$n_p \sim (\Delta w_{tot})^2,$$

which ultimately would lead to the breakdown of the method for long real-time computations. To overcome this limitation, a procedure must obviously be devised for keeping the weight spreading to an acceptable level.

G. Weight Spreading Reduction Scheme

We propose here a first practical procedure for limiting the weight spreading. Instead of simply discarding the terms in the weight equations that ensured that definitions (16)–(22) are preserved, let us attempt to replace them by numerically less demanding ones, which approximately have the same effect. Coming back to our initial physical system, a possible scheme would be to write (25) and (23) with the additional terms

$$\frac{d}{dt}w_i(t) = -p_i(t)\frac{C[\delta f, f_{\rm M}]}{f_{\rm M}} - \eta\,[w_i - W(\boldsymbol{v}_i;t)], \tag{40}$$

$$\frac{d}{dt}p_i(t) = -\eta\,[p_i - P(\boldsymbol{v}_i;t)], \tag{41}$$

which provide a continuous relaxation of w_i and p_i towards their average values $W(\boldsymbol{v}_i;t)$ and $P(\boldsymbol{v}_i;t)$ with a given rate η. It is easy to validate (40)–(41) by adjusting Eq. (26) for this new evolution of weights and showing that one still recovers the correct equations for δf, $f_{\rm SM}$ by taking the moments $\int w\,dw\,dp$, $\int p\,dw\,dp$.

Implementing Eqs (40)–(41) nonetheless requires evaluating the average fields $W(\boldsymbol{v};t)$ and $P(\boldsymbol{v};t)$ at each time step, which may still tend to be relatively costly. In practice, the algorithm we have adopted for reducing the weight spreading therefore took the simplest form, which consists in reassigning the weights to their average value only periodically in time. This corresponds to a discontinuous reduction, allowing for a limited spreading between consecutive applications of this operation.

In general, to compute the average weight fields $W(\boldsymbol{z})$ and $P(\boldsymbol{z})$, phase space $\boldsymbol{z} = (\boldsymbol{x}, \boldsymbol{v})$ is partitioned into a set of bins ΔV (see Fig. 1b) with dimensions relatively small compared to the characteristic physical length. In each of these cells, W and P must be evaluated statistically. We will restrict the discussion here to the computation of W, all following relations having their direct analogue for P.

As the computed field W is used for reassigning the particle weights w_i, one may want to ensure that certain moments of δf are preserved through this weight spread reduction scheme. Using the notation w_i and w_i' for the weights just before and just after this procedure was applied, respectively, the conservation within a given bin ΔV of, for instance, particle number and momentum in δf appears as

$$\sum_{i=1}^{n_b} w_i = \sum_{i=1}^{n_b} w_i' = \sum_{i=1}^{n_b} W(\boldsymbol{z}_i), \tag{42}$$

$$\sum_{i=1}^{n_b} w_i \boldsymbol{v}_i = \sum_{i=1}^{n_b} w_i' \boldsymbol{v}_i = \sum_{i=1}^{n_b} W(\boldsymbol{z}_i)\, \boldsymbol{v}_i. \tag{43}$$

This may be achieved by considering a fit for $W(\boldsymbol{z})$, within each cell, of the form

$$W(\boldsymbol{v}) = W_0 + \boldsymbol{W}_1 \cdot \boldsymbol{v}/v_{\text{th}}. \tag{44}$$

Inserting (44) into (42)–(43) gives

$$W_0\, n_b + \frac{\boldsymbol{W}_1}{v_{\text{th}}} \cdot \sum_{i=1}^{n_b} \boldsymbol{v}_i = \sum_{i=1}^{n_b} w_i, \tag{45}$$

$$W_0 \sum_{i=1}^{n_b} \boldsymbol{v}_i + \frac{\boldsymbol{W}_1}{v_{\text{th}}} \cdot \sum_{i=1}^{n_b} \boldsymbol{v}_i\, \boldsymbol{v}_i = \sum_{i=1}^{n_b} w_i\, \boldsymbol{v}_i. \tag{46}$$

It can easily be shown, that this linear system of equations for the parameters W_0 and $\boldsymbol{W}_1$ is equivalent to applying a standard regression, which minimizes the sum of squared differences $\sum [W(\boldsymbol{v}_i) - w_i]^2$ for the fit (44). It is straightforward to generalize this method to ensure conservation of additional quantities. For instance, kinetic energy may also be taken account of by carrying out a regression using the fit

$$W(\boldsymbol{v}) = W_0 + \boldsymbol{W}_1 \cdot \boldsymbol{v}/v_{\text{th}} + W_2\, (v/v_{\text{th}})^2.$$

For the reduction scheme to actually correct the weights within a given bin, that is $w_i' = W(\boldsymbol{z}_i) \neq w_i$, the number n_b of particles must at least be greater than the number N of quantities that are to be conserved. From this naturally follows a certain requirement on the minimum number n_p of total particles to be used in a given simulation. Note, however, that by increasing N one may consider larger bins, as the corresponding fit for W includes more structure. In regions of phase space with few marker particles, one may always have cells such that $n_b < N$. In such bins the system of equations (45)–(46) is undetermined and no weight reassignment is carried out. Nonetheless, through collisions all particles from time to time end up in more densely populated regions and thus undergo correction. Thus, even if the weight spread reduction is carried out over a limited region, one achieves a reduction of $\Delta w_{\boldsymbol{z}}$ over the whole phase space $\boldsymbol{z}$.

H. Illustrations

To actually illustrate some of the points made in the previous sections, some results are presented here of δf simulations carried out for solving equation (3). Hence, marker particles have been evolved according to Eqs (13)–(15), (25), and (23), together with the weight spread reduction scheme presented in Sec. II G. In carrying out these simulations, the operator $C[\delta f, f_{\mathrm{M}}]$ appearing in the weight equation (25), describing collisions of the background particles off of δf, has been replaced by the simpler operator proposed by Lin *et al.*:[10]

$$C[\delta f, f_{\mathrm{M}}]/f_{\mathrm{M}} \simeq \mathcal{O}\delta f = \frac{6\sqrt{\pi}}{v_{\mathrm{th}}}\,\boldsymbol{\mathcal{P}}(\delta f)\boldsymbol{\cdot} H\,\frac{\boldsymbol{v}}{v_{\mathrm{th}}} + \frac{\sqrt{\pi}}{v_{\mathrm{th}}^2}\,\mathcal{E}(\delta f)\left[2(\frac{v}{v_{\mathrm{th}}})^2 H - H - K\right], \tag{47}$$

$$\boldsymbol{\mathcal{P}}(\delta f) = -\int C[f_{\mathrm{M}}, \delta f]\,\boldsymbol{v}\,d\boldsymbol{v} = \sum_{i=1}^{n_p} w_i \frac{d\boldsymbol{v}_i}{dt}, \tag{48}$$

$$\mathcal{E}(\delta f) = -\int C[f_{\mathrm{M}}, \delta f]\,v^2\,d\boldsymbol{v} = \sum_{i=1}^{n_p} w_i \frac{d(\boldsymbol{v}_i{}^2)}{dt}, \tag{49}$$

where $H = H(v/v_{\mathrm{th}})$, $K = K(v/v_{\mathrm{th}})$ are again given by (11)–(12), and $d\boldsymbol{v}_i/dt$, $d(\boldsymbol{v}_i{}^2)/dt$ are the variation in time of momentum and kinetic energy of marker particles due to test particle collisions off of the background [as given by (13)–(15)]. In (47), δf appears only through the parameters $\boldsymbol{\mathcal{P}}$ and $\mathcal{E}$, and therefore $f_{\mathrm{M}}\mathcal{O}\delta f$ is significantly simpler to evaluate for different values of $\boldsymbol{v}$ than with the full operator, which is of the more general integral form: $C[\delta f, f_{\mathrm{M}}] = \int K(\boldsymbol{v}', \boldsymbol{v})\delta f(\boldsymbol{v}')d\boldsymbol{v}'$ [see (2)]. Relation (47) is an improvement over the approximation considered in Refs. 8 and 9, as it not only ensures that the linearized collision operator $\widehat{C}\delta f \simeq C[f_{\rm M}, \delta f] + f_{\rm M}\mathcal{O}\delta f$ still conserves the collision invariants (particle number, momentum, kinetic energy), but also that it still annihilates functions of the form (4). This last point is proven in appendix A. Also shown in Appendix A are the modifications to (37) and (38) when applying approximation (47).

For the following results, the initial marker particle distribution (27) was chosen such that both δf and g have already reached relaxed states, that is, $\delta f(t=0)$ was taken of the form (4), with $c_0 = 0$, $\boldsymbol{c}_1 = \boldsymbol{e}_z$, $c_2 = 1$, and $g(t=0) = n_p f_{\rm M}$ with $n_p = 10^4$. This choice allows one to test the stability of the algorithm for maintaining δf, and to clearly show the continuing evolution of $F(\boldsymbol{v}, w, p; t)$ in the extended phase space related to the spreading of Δw and Δp. This is a computation similar to the one shown in Fig. 8 of reference 4 however over a significantly larger number of collision times $\tau = \overline{\nu}^{-1}$.

Marker particles have been evolved with a time step $\Delta t = 10^{-2}\tau$ in the three-dimensional velocity space using Cartesian coordinates (v_x, v_y, v_z). However, when reconstructing δf or the weight field W, we have taken advantage of the symmetry of the solution around the direction $\boldsymbol{c}_1 = \boldsymbol{e}_z$. Thus, for this specific purpose, cylindrical coordinates $(v_\perp, \varphi, v_z)$ were used.

Figures 2a and 2b present the average weight field $W(v_\perp, v_z; t)$ along v_z for fixed $v_\perp = 1.2 v_{\rm th}$ after one hundred collision times, i.e., $t = 100\,\tau$. Figure 2a shows the final state without having applied the weight spread reduction scheme, while in figure 2b this procedure was applied every collision time τ, i.e., every hundred time steps Δt. A Cartesian grid in the space $(v_\perp, v_z)$ with mesh size $\Delta v_\perp = \Delta v_z = 0.4\, v_{\rm th}$ defined the bins used for reconstructing W. The boundaries of these bins are pointed out with dotted vertical lines. The root mean square deviation of weights w_i within each bin, giving an estimate for the spreading Δw, is represented in figures 2a and 2b by the dashed curves $W \pm \Delta w$. At the end of the run, when not making use of the weight spread reduction scheme, Δw has become of the same order as the average field W, which thus fluctuates significantly around the exact solution $W_{\rm exact} = c_0 + \boldsymbol{c}_1 \cdot \boldsymbol{v}/v_{\rm th} + c_2(v/v_{\rm th})^2$ represented by the dash-dotted curve. When applying the reduction procedure, the fluctuation level is clearly reduced. Figure 2b shows the state just after the reduction procedure was applied for the last time. Thus, the small but non-zero estimate of Δw appearing in this plot is essentially an artifact of the variation of $W(\boldsymbol{v})$ within the finite size bins. The slight deviations appearing for $|v_z| \gtrsim 2.5\, v_{\rm th}$ are due to the lower density of marker particles in this region of velocity space. It will be shown in Sec. III how, by adding sources and sinks, a higher density of marker particles can be maintained in the tails of the distribution and therefore a better resolution obtained.

The quantitative evaluation of weight spreading and associated level of field fluctuations is presented in figures 3a and 3b. Figure 3a shows the linear increase in time of the entropy $\mathcal{S}_w(t)$ in the absence of weight spread reduction, which corresponds [see (35)] to a linear increase of $(\Delta w_{\rm tot})^2$. The rate is in good agreement with relation (A4), giving in this case the prediction $d\mathcal{S}_w/dt = 6.6 \cdot 10^{-5}\, \overline{\nu}$. When applying the reduction scheme, $\mathcal{S}_w(t)$ adopts a sawtooth-like behavior, as it periodically starts to grow linearly before being reduced, every collision period τ, to its initial value $\mathcal{S}_w(t=0) = \mathcal{F} = (1/2) \int d\boldsymbol{v}\, \delta f^{\,2}/n_p f_{\rm M} = 8 \cdot 10^{-4}$. For the simulation without the reduction procedure, the drift of $\mathcal{S}_w$ from $\mathcal{F}$ at the end of the run is approximately hundred times greater than at its successive peaks in the case including the scheme. This corresponds, according to (35), to a spreading Δw already ten times larger than the average one maintained in the latter case. The fluctuation of the field δf around its exact stationary state $\delta f_{\rm exact} = \delta f(t=0)$, is clearly shown in figure 3b, where the deviation is estimated in time using

$$[\Delta(\delta f)]^2 = \frac{\int (\delta f - \delta f_{\rm exact})^2\, d\boldsymbol{v}}{\int (\delta f_{\rm exact})^2\, d\boldsymbol{v}}.$$

The initial deviation, common for both the cases with and without the reduction, is due to the standard sampling noise mentioned in Sec. II E, while the subsequent, basically linear increase in time for the run without reduction is related to the evolution of ${\Delta w_{\rm tot}}^2 \sim t$.

Finally, Fig. 4 illustrates the necessity in some situations of applying higher order regressions for reconstructing W in the reduction procedure, as described in Sec.II G. By taking the lowest order fit, where $W(\boldsymbol{v})$ is approximated as a constant W_0 in each bin, total momentum along Oz is manifestly not conserved. For this particular case, it can in fact be shown that the errors due to the finite size of the bins systematically add up. The next-order scheme, which involves the regression $W(\boldsymbol{v}) = W_0 + W_{1\perp} v_\perp / v_{\mathrm{th}} + W_{1z} v_z / v_{\mathrm{th}}$ within each bin, and thus conserves momentum along $v_\perp$ as well as v_z, clearly removes this problem. A second-order regression, ensuring also conservation of kinetic energy, turned out not to be necessary in this case.

III. EVOLVING THE BACKGROUND IN THE δf ALGORITHM

A. Derivation of a Self-Consistent Set of Fluid and Marker Particle Equations for the Simultaneous Evolution of a Maxwellian Background and δf

The methods developed in Sec. II will now be used as a basis for carrying out simulations of driven plasmas. If the system is submitted to the drive for a sufficiently long time, the whole distribution will evolve significantly from its initial state. In a δf simulation, this requires evolving the background, so that it remains a good approximation of the distribution at all times. Indeed, the average of the ratio $|\delta f/f|$ over phase space must remain small throughout the run[1,6] for the δf approach to be applied advantageously in such a situation. For the cases considered here, self-collisions are assumed important, so that a natural choice for the shape of the background is a shifted Maxwellian distribution:

$$f = f_{\mathrm{SM}} + \delta f, \tag{50}$$

$$f_{\mathrm{SM}}[\boldsymbol{v}; N(\boldsymbol{x};t), \boldsymbol{u}(\boldsymbol{x};t), T(\boldsymbol{x};t)] = \frac{N(\boldsymbol{x};t)/\overline{N}}{[2\pi T(\boldsymbol{x};t)/m]^{3/2}} \exp\left(-\frac{1}{2}\frac{[\boldsymbol{v}-\boldsymbol{u}(\boldsymbol{x};t)]^2}{T(\boldsymbol{x};t)/m}\right), \tag{51}$$

where the density N, average velocity $\boldsymbol{u}$ and temperature T are in general all functions of position $\boldsymbol{x}$ and time t. The notation $\overline{N}$ is used for the average density. The evolution of the background thus arises through these parameters. Their evolution in turn is governed by a set of fluid equations, with correct closure through moments of δf, so as to maintain a specified separation between the two components f_{SM} and δf. It will be shown shortly how these fluid equations can be derived systematically from the equation for δf once appropriate constraints defining this separation have been chosen.

In view of the following illustrations, where systems submitted to a constant drive are studied, it is appropriate to consider the set of constraints

$$\int \delta f \, \boldsymbol{v}^{\,j} \, d\boldsymbol{v} = 0, \qquad j = 0, 1, 2. \tag{52}$$

With this separation at each point $\boldsymbol{x}$, density, momentum and kinetic energy of the full distribution f are all contained in the background f_{SM}.

Before carrying on, let us stress the fact that the decomposition defined by (50), (51) and (52) is not necessarily adapted for all cases and as a consequence no recipe, which is both general and practical, can be given for evolving the background. For instance, if one intended to simulate a system with different time and length scales, as in the case of microturbulence-driven transport, the separation might be fixed by defining the fluid-like background as

$$\overline{f} = \langle f \rangle_{\boldsymbol{x};t},$$

where the average is taken over the faster length and time scales. Nonetheless, the derivation presented below should provide the spirit for tailoring equations for other specific problems.

Let us now start by considering the Fokker–Planck equation for a distribution of electrons submitted to electromagnetic fields $(\boldsymbol{E}, \boldsymbol{B})$:

$$\frac{\partial f}{\partial t} + \boldsymbol{v}\cdot\frac{\partial f}{\partial \boldsymbol{x}} + \frac{(-e)}{m}(\boldsymbol{E} + \boldsymbol{v} \times \boldsymbol{B})\cdot\frac{\partial f}{\partial \boldsymbol{v}} = -\left\{ C_{ee}[f, f] + C_{ei} f \right\}, \tag{53}$$

where C_{ee} stands for the Landau operator (2) representing self-collisions between electrons and

$$C_{ei} = -\overline{\nu}_{ei}\, v_{\text{th}}^3 \,\frac{\partial}{\partial \boldsymbol{v}}\cdot\mathsf{U}(\boldsymbol{v})\cdot\frac{\partial}{\partial \boldsymbol{v}} \tag{54}$$

is the Lorentz collision operator describing collisions of electrons off of ions, with $\overline{\nu}_{ei} = e^2 N_i (Ze)^2 \ln\Lambda / 8\pi\, \epsilon_0^2\, m^2\, v_{\text{th}}^3$. Ions are assumed to be immobile in the considered frame of reference and their density given by N_i. To lighten notations, all physical quantities relative to electrons are not explicitly labeled as such. Although the numerical results presented in this paper are only for homogeneous plasmas driven by an electric field, these simplifications have not yet been made in (53), so as to nonetheless ensure a minimum of generality for the next derivation.

By applying decomposition (50), the equation for δf can be written:

$$\frac{D}{Dt}\delta f = -\left\{ \frac{D}{Dt} f_{\text{SM}} + C_{ee}[\delta f, f_{\text{SM}}] \right\}, \tag{55}$$

$$\frac{D}{Dt} = \frac{\partial}{\partial t} + \boldsymbol{v}\cdot\frac{\partial}{\partial \boldsymbol{x}} + \frac{(-e)}{m}(\boldsymbol{E} + \boldsymbol{v} \times \boldsymbol{B})\cdot\frac{\partial}{\partial \boldsymbol{v}} + C_{ee}[f_{\text{SM}}, \ ] + C_{ei}. \tag{56}$$

To obtain (55), the full nonlinear operator $C_{ee}[f,f]$ was again replaced by $\widehat{C} = C[f_{\rm SM}, \delta f] + C[\delta f, f_{\rm SM}]$. This approximation should be all the more justified here, as the background $f_{\rm SM}$ is now being evolved so as to keep δf small.

When considering the set of constraints (52), the equations for the background parameters $(N, \boldsymbol{u}, T)$ can be derived by taking the velocity moments $\overline{N}\int d\boldsymbol{v}$, $\overline{N}\int d\boldsymbol{v}\,\boldsymbol{v}$ and $\overline{N}\int d\boldsymbol{v}\,v^2$ of the equation (55) for δf and by making use of (52). This leads to the set of fluid equations[17]

- Continuity equation:

$$\frac{\partial N}{\partial t} + \frac{\partial}{\partial \boldsymbol{x}}\cdot(N\boldsymbol{u}) = 0. \tag{57}$$

- Momentum equation:

$$\begin{aligned} m\,N\left(\frac{\partial \boldsymbol{u}}{\partial t} + \boldsymbol{u}\cdot\frac{\partial \boldsymbol{u}}{\partial \boldsymbol{x}}\right) &= -\frac{\partial}{\partial \boldsymbol{x}}(N\,T) - \frac{\partial}{\partial \boldsymbol{x}}\cdot\Pi(\delta f) \\ &\quad + (-e)N\,(\boldsymbol{E} + \boldsymbol{u}\times\boldsymbol{B}) + \boldsymbol{R}_{ei}(f_{\rm SM}) + \boldsymbol{R}_{ei}(\delta f). \end{aligned} \tag{58}$$

- Heat equation:

$$\frac{\partial}{\partial t}\left(\frac{3}{2}N\,T + \frac{1}{2}m\,N\,u^2\right) + \frac{\partial}{\partial \boldsymbol{x}}\cdot\left[\frac{5}{2}N\,T\,\boldsymbol{u} + \frac{1}{2}m\,N\,u^2\,\boldsymbol{u} + \Pi\cdot\boldsymbol{u} + \boldsymbol{q}\,(\delta f)\right] = (-e)N\boldsymbol{u}\cdot\boldsymbol{E}. \tag{59}$$

Note that the above fluid equations are closed through the following moments of δf:

$$\begin{aligned} \Pi(\delta f) &= m\overline{N}\int\left[(\boldsymbol{v}-\boldsymbol{u})\,(\boldsymbol{v}-\boldsymbol{u}) - \frac{1}{3}(\boldsymbol{v}-\boldsymbol{u})^2\mathbf{1}\right]\delta f\,d\boldsymbol{v} = m\overline{N}\int \boldsymbol{v}\,\boldsymbol{v}\,\delta f\,d\boldsymbol{v} \quad \text{(stress tensor)}, \\ \boldsymbol{R}_{ei}(\delta f) &= -m\overline{N}\int \boldsymbol{v}\,C_{ei}\delta f\,d\boldsymbol{v} \quad \text{(drag of } \delta f \text{ on ions)}, \\ \boldsymbol{q}\,(\delta f) &= \frac{m}{2}\overline{N}\int(\boldsymbol{v}-\boldsymbol{u})^2(\boldsymbol{v}-\boldsymbol{u})\,\delta f\,d\boldsymbol{v} = \frac{m}{2}\overline{N}\int(\boldsymbol{v}-\boldsymbol{u})^2\boldsymbol{v}\,\delta f\,d\boldsymbol{v} \quad \text{(heat flux in } \delta f), \end{aligned}$$

where the second equalities for $\Pi(\delta f)$ and $\boldsymbol{q}\,(\delta f)$ were obtained by invoking the set of constraints (52). The drag $\boldsymbol{R}_{ei}(f_{\rm SM})$ of the Maxwellian background off of the ions can be expressed in terms of the Rosenbluth potential (11):

$$\boldsymbol{R}_{ei}(f_{\rm SM}) = -m\overline{N}\int \boldsymbol{v}\, C_{ei} f_{\rm SM}\, d\boldsymbol{v} = -2\,\overline{\nu}_{ei}\, m\, N\, v_{\rm th} H(u/v_{\rm th})\, \boldsymbol{u}/v_{\rm th}. \tag{60}$$

For completeness, let us still derive equations for the marker particles representing δf. We will again choose for the marker particle distribution $g(\boldsymbol{x}, \boldsymbol{v}; t)$ in the physical phase space $(\boldsymbol{x}, \boldsymbol{v})$ the equation

$$\frac{D}{Dt} g = 0, \tag{61}$$

where now D/Dt is given by (56). Similarly as in Sec. II, the equations of motion in the extended phase space $(\boldsymbol{x}, \boldsymbol{v}, w, p)$ for the marker particles representing δf can then be derived from (55) and (61) to give

$$\frac{d\boldsymbol{x}(t)}{dt} = \boldsymbol{v}, \tag{62}$$

$$\frac{d\boldsymbol{v}(t)}{dt} = -\frac{e}{m}(\boldsymbol{E} + \boldsymbol{v} \times \boldsymbol{B}) + \boldsymbol{a}_{ee} + \boldsymbol{a}_{ei}, \tag{63}$$

$$\dot{w} \doteq \frac{dw(t)}{dt} = -\frac{p}{f_{\rm SM}} \left\{ \frac{D}{Dt} f_{\rm SM} + C_{ee}[\delta f, f_{\rm SM}] \right\}, \tag{64}$$

$$\dot{p} \doteq \frac{dp(t)}{dt} = \frac{p}{f_{\rm SM}} \frac{D}{Dt} f_{\rm SM}, \tag{65}$$

having discarded, as usual, unpractical terms relative to diffusive processes when deriving the weight equations (64) and (65), which leads to the spreading of w and p. Here $\boldsymbol{a}_{ee}$ and $\boldsymbol{a}_{ei}$ stand for the random accelerations relative to test-particle collisions off of the shifted Maxwellian background $f_{\rm SM}$ and the immobile ions respectively.

The Fokker–Planck equation for the distribution $F(\boldsymbol{x}, \boldsymbol{v}, w, p; t)$ of marker particles in the extended phase space $(\boldsymbol{x}, \boldsymbol{v}, w, p)$ can thus be written

$$\frac{D}{Dt} F + \frac{\partial}{\partial w}(\dot{w} F) + \frac{\partial}{\partial p}(\dot{p}\, F) = 0, \tag{66}$$

with the initial condition

$$F(\boldsymbol{x}, \boldsymbol{v}, w, p; t = 0) = g_0(\boldsymbol{x}, \boldsymbol{v})\, \delta(w - W_0(\boldsymbol{x}, \boldsymbol{v}))\, \delta(p - P_0(\boldsymbol{x}, \boldsymbol{v})), \tag{67}$$

with $W_0(\boldsymbol{x}, \boldsymbol{v}) = \delta f(\boldsymbol{x}, \boldsymbol{v}; t = 0)/g_0(\boldsymbol{x}, \boldsymbol{v})$ and $P_0(\boldsymbol{x}, \boldsymbol{v}) = f_{\rm SM}(\boldsymbol{x}, \boldsymbol{v}; t = 0)/g_0(\boldsymbol{x}, \boldsymbol{v})$. One can again easily show that by identifying

$$g(\boldsymbol{x}, \boldsymbol{v}; t) = \int dw\, dp\, F(\boldsymbol{x}, \boldsymbol{v}, w, p; t), \tag{68}$$

$$f_{\rm SM}(\boldsymbol{x}, \boldsymbol{v}; t) = \int dw\, dp\, p\, F(\boldsymbol{x}, \boldsymbol{v}, w, p; t), \tag{69}$$

$$\delta f(\boldsymbol{x}, \boldsymbol{v}; t) = \int dw\, dp\, w\, F(\boldsymbol{x}, \boldsymbol{v}, w, p; t) \tag{70}$$

and taking the equivalent moments of (66) and (67), one indeed recovers the equation (55) for δf, which is the proof for the validity of (62)–(65).

The simultaneous evolution of the marker particle equations (62)–(65) for solving the equation (55) for δf, together with the set of fluid equations (57)–(59) for the background parameters $(N, \boldsymbol{u}, T)$ theoretically ensures that the set of constraints (52) are verified.

B. First Illustration: Electrical Spitzer Conductivity

We will consider here a homogeneous, neutral plasma of electrons and a single species of immobile ions submitted to a constant uniform electric field $\boldsymbol{E}$. By assuming a homogeneous system, the physical phase space is again reduced to velocity space $\boldsymbol{v}$. Hence, the Fokker–Planck equation (53) simplifies to:

$$\frac{\partial f}{\partial t} + \frac{(-e)}{m}\boldsymbol{E}\cdot\frac{\partial f}{\partial \boldsymbol{v}} = -\left\{ C_{ee}[f, f] + C_{ei} f \right\}. \tag{71}$$

In particular, solving this equation in the linear limit of a weak electric field enables one to recover the electrical Spitzer conductivity.[18]

Applying the δf approach with evolving Maxwellian background developed in Sec. III A, one can make direct use of the set of fluid equations (57)–(59) for the background parameters, and the equations of motion (63)–(65) for the marker particles in the extended phase space $(\boldsymbol{v}, w, p)$. Thus, the equations for the parameters $[N(t), \boldsymbol{u}(t), T(t)]$, which are now only time dependent, are given by

$$\frac{dN}{dt} = 0, \quad \Longrightarrow \quad N(t) = \overline{N} = \text{const.}, \tag{72}$$

$$m\frac{d\boldsymbol{u}}{dt} = -e\boldsymbol{E} + \frac{1}{\overline{N}}\left[\boldsymbol{R}_{ei}(f_{\rm SM}) + \boldsymbol{R}_{ei}(\delta f)\right], \tag{73}$$

$$\frac{d}{dt}(\frac{3}{2}T + \frac{1}{2}m\, u^2) = -e\, \boldsymbol{u}\cdot\boldsymbol{E} \tag{74}$$

and the equations for the marker particles

$$\frac{d\boldsymbol{v}}{dt} = -\frac{e}{m}\boldsymbol{E} + \boldsymbol{a}_{ee} + \boldsymbol{a}_{ei}, \tag{75}$$

$$\frac{dw}{dt} = -\frac{p}{f_{\mathrm{SM}}}\left\{\frac{D}{Dt}f_{\mathrm{SM}} + C_{ee}[\delta f, f_{\mathrm{SM}}]\right\} + \alpha w, \tag{76}$$

$$\frac{dp(t)}{dt} = \frac{p}{f_{\mathrm{SM}}}\frac{D}{Dt}f_{\mathrm{SM}} + \alpha p. \tag{77}$$

Here we have implemented the method for adding sources and sinks of marker particles in conjunction with the weight spread reduction scheme as described in appendix B. This accounts for the terms in (76) and (77) proportional to the annihilation rate α of marker particles. Annihilated particles are immediately reinjected with zero weights, randomly and uniformly on a shell $v_{\min} < |\boldsymbol{v} - \boldsymbol{u}| < v_{\max}$, where $v_{\min/\max}$ are typically of the order of a few v_{th}. This enables one to maintain a good resolution in the tail of the distribution f, as the marker particles, through collisions on f_{SM}, tend to diffuse down onto the bulk.

The term Df_{SM}/Dt appearing in (76) and (77) can be written more explicitly by applying definition (56) of the operator D/Dt in the particular case considered here:

$$\begin{aligned}\frac{1}{f_{\mathrm{SM}}}\frac{D}{Dt}f_{\mathrm{SM}} &= \frac{d\ln T}{dt}\left[\frac{(\boldsymbol{v}-\boldsymbol{u})^2}{2{v_{\mathrm{th}}}^2} - \frac{3}{2}\right] + \left[\frac{d\boldsymbol{u}}{dt} - \frac{(-e)}{m}\boldsymbol{E}\right]\cdot\frac{(\boldsymbol{v}-\boldsymbol{u})}{{v_{\mathrm{th}}}^2} + \frac{1}{f_{\mathrm{SM}}}C_{ei}f_{\mathrm{SM}} \\ &= \frac{1}{m\overline{N}v_{\mathrm{th}}}\left[\boldsymbol{R}_{ei}(f_{\mathrm{SM}}) + \boldsymbol{R}_{ei}(\delta f)\right]\cdot\left[\frac{\boldsymbol{v}}{v_{\mathrm{th}}} - \frac{(\boldsymbol{v}-\boldsymbol{u})^2}{3{v_{\mathrm{th}}}^2}\frac{\boldsymbol{u}}{v_{\mathrm{th}}}\right] \\ &\quad -\nu_{ei}(v)\left\{\left[1 + \left(\frac{uv}{{v_{\mathrm{th}}}^2}\right)^2\right] - \left[1 + \frac{\boldsymbol{u}\cdot\boldsymbol{v}}{{v_{\mathrm{th}}}^2}\right]^2\right\},\end{aligned} \tag{78}$$

having made use of Eqs. (54), (73), and (74), as well as the definition $\nu_{ei}(v) = \overline{\nu}_{ei}/(v/v_{\mathrm{th}})^3$.

Let us now make some comments on how the above equations are actually solved. Integrating (75) over a time step Δt requires computing random velocity increments $\Delta\boldsymbol{v}_{ee}$ related to the scattering off of the shifted Maxwellian background f_{SM}, as well as increments $\Delta\boldsymbol{v}_{ei}$ related to collisions off of the ions. For $\Delta\boldsymbol{v}_{ee}$, one can directly apply relations (13)–(15) by going into the frame of reference moving with the average velocity $\boldsymbol{u}$ of the background. In the ion frame, the increment $\Delta\boldsymbol{v}_{ei}$, which in particular must be such as to conserve kinetic energy, is expressed in terms of the random scattering angle θ and random azimuthal angle ϕ:[19]

$$\Delta v_{x,\,ei} = \frac{1}{v_\perp}\left[v_x v_z \sin\theta\cos\phi - v_y v \sin\theta\sin\phi + v_x v_\perp(\cos\theta - 1)\right], \tag{79}$$

$$\Delta v_{y,\,ei} = \frac{1}{v_\perp}\left[v_y v_z \sin\theta\cos\phi + v_x v \sin\theta\sin\phi + v_y v_\perp(\cos\theta - 1)\right], \tag{80}$$

$$\Delta v_{z,\,ei} = -v_\perp \sin\theta\cos\phi + v_z(\cos\theta - 1), \tag{81}$$

with $\boldsymbol{v}(t) = v_x\boldsymbol{e}_x + v_y\boldsymbol{e}_y + v_z\boldsymbol{e}_z$ being the incoming velocity, $v = |\boldsymbol{v}|$ and $v_\perp^2 = v_x^2 + v_y^2$. The angle ϕ is taken from a random uniform distribution over $[0, 2\pi]$ and

$$\theta = 2\sqrt{\nu_{ei}(v)\Delta t}\, R, \tag{82}$$

where R is a random number with zero mean and unit rms width. By averaging over all the particles, one can show that (79)–(81) correctly reproduces the Lorentz operator.

The operator $C_{ee}[\delta f, f_{\rm SM}]$ appearing in (76) is again approximated with $f_{\rm SM}\mathcal{O}\delta f$ given by equations (47)–(49), which must now be transformed from the frame moving with the average velocity $\boldsymbol{u}$ of the background back to the lab frame, giving

$$C[\delta f, f_{\rm SM}]/f_{\rm SM} \simeq \mathcal{O}\delta f = \frac{6\sqrt{\pi}}{v_{\rm th}}\boldsymbol{\mathcal{P}}(\delta f)\boldsymbol{\cdot} H\frac{(\boldsymbol{v}-\boldsymbol{u})}{v_{\rm th}} + \frac{\sqrt{\pi}}{{v_{\rm th}}^2}\mathcal{E}(\delta f)\left[2\frac{(\boldsymbol{v}-\boldsymbol{u})^2}{{v_{\rm th}}^2}H - H - K\right], \tag{83}$$

$$\boldsymbol{\mathcal{P}}(\delta f) = -\int C[f_{\rm M}, \delta f]\,(\boldsymbol{v}-\boldsymbol{u})\,d\boldsymbol{v} \;=\; \sum_{i=1}^{n_p} w_i\frac{d\boldsymbol{v}_i}{dt_{ee}}, \tag{84}$$

$$\mathcal{E}(\delta f) = -\int C[f_{\rm M}, \delta f]\,(\boldsymbol{v}-\boldsymbol{u})^2\,d\boldsymbol{v} \;=\; \sum_{i=1}^{n_p} w_i\frac{d({\boldsymbol{v}_i}^2)}{dt_{ee}} - 2\boldsymbol{u}\boldsymbol{\cdot}\sum_{i=1}^{n_p} w_i\frac{d\boldsymbol{v}_i}{dt_{ee}}, \tag{85}$$

where d/dt_{ee} stands for the variation due to scattering off of the background, and here $H = H(|\boldsymbol{v}-\boldsymbol{u}|/v_{\rm th})$, $K = K(|\boldsymbol{v}-\boldsymbol{u}|/v_{\rm th})$.

To avoid having to deal with the singularity of $\nu_{ei}(v)$ at $v = 0$, the above equations were implemented by taking

$$\nu_{ei}(v) = \begin{cases} \overline{\nu}_{ei}/(v/v_{\rm th})^3 & \text{for } \; v > v_c, \\ 0 & \text{otherwise,} \end{cases}$$

where v_c was chosen such that the fraction of electrons within the sphere $v < v_c$ was sufficiently small so as to not affect the simulation. One can give a physical meaning to v_c by typically taking $v_c \sim v_{\rm th}\sqrt{m/m_i} \sim \boldsymbol{v}_{{\rm th},\,i}$ assuming $T_i \sim T$. To ensure that the system of fluid and marker particle equations further conserves the separation defined by the constraints

(52), this approximation on $\nu_{ei}(v)$ has to be applied at all levels of the computation, that is, when scattering the particles according to (79)–(82), when integrating the weight equations using relation (78) for $Df_{\rm SM}/Dt$, and finally, when computing the drag $\boldsymbol{R}_{ei}(f_{\rm SM})$ of $f_{\rm SM}$ on ions, which instead of (60) is now

$$\boldsymbol{R}_{ei}(f_{\rm SM}) = -2\frac{\overline{\nu}_{ei} m \overline{N} v_{\rm th}}{(u/v_{\rm th})^3}\left\{\frac{1}{2}\left[\operatorname{erf}\left(\frac{u-v_c}{\sqrt{2}v_{\rm th}}\right)+\operatorname{erf}\left(\frac{u+v_c}{\sqrt{2}v_{\rm th}}\right)\right]\right.$$
$$\left. - \sqrt{\frac{2}{\pi}}\left(\frac{2v_c}{v_{\rm th}}\right)^{-1}\left[\exp -\frac{(u-v_c)^2}{2{v_{\rm th}}^2} - \exp -\frac{(u+v_c)^2}{2{v_{\rm th}}^2}\right]\right\}\frac{\boldsymbol{u}}{v_{\rm th}}.$$

This last relation naturally reduces to (60) in the limit $v_c \to 0$.

Finally, the drag of δf off of the ions can be computed conveniently by using a relation similar to (84)–(85):

$$\boldsymbol{R}_{ei}(\delta f) = m\overline{N}\sum_{i=1}^{n_p} w_i \frac{d\boldsymbol{v}_i}{dt_{ei}},$$

where $d\boldsymbol{v}_i/dt_{ei}$ stands for the variation in time of momentum due to test-particle collisions off of the ions, as given by (79)–(81).

1. Results for Spitzer Conductivity

To benchmark the δf simulation with evolving background, we started by considering a high electrical field $E = 5\cdot 10^{-2}\, m\overline{\nu}_{ee}(0)v_{\rm th}(0)/e$, which is of the order of the thermal runaway field $E_c = 0.11\, m\overline{\nu}_{ee}v_{\rm th}/e$. Here $\overline{\nu}_{ee} = \overline{N}e^4\ln\Lambda/2\pi\epsilon_0^2 m^2 v_{\rm th}^3$ is the thermal electron–electron collision frequency and $\overline{\nu}_{ee}(0)$ is its value for the initial temperature. Considering a strong drive enabled us to easily compare results with those obtained from a particle in cell (PIC) computation. The PIC code was written using the collision model developed by Takizuka and Abe[19] for implementing self collisions, which reproduces the full nonlinear collision operator.

The results for runs carried out over a time $t = 70\,\overline{\nu}_{ee}(0)^{-1}$ are given in Fig. 5. The degree of ionization of ions was chosen $Z = 1$, the time step $\Delta t = 10^{-2}\overline{\nu}_{ee}(0)^{-1}$, and the number of particles $n_p = 10^4$. Initially, $\delta f \equiv 0$, so that the full distribution at time $t = 0$

is given by the background $f_{\rm SM}(t = 0)$, which is plotted in Fig. 5b. The evolution of temperature T and average velocity $\boldsymbol{u}$ ($\sim$ current) are given in Fig. 5a. Besides the δf and PIC simulations, Fig. 5a also represents, for comparison, the so-called fluid result. The fluid calculation corresponds to solving the fluid equations (72)–(74) by neglecting the closure term $\boldsymbol{R}_{ei}(\delta f)$, which describes the evolution where the distribution is constrained to remain a Maxwellian. Due to the fact that there is a significant fraction of runaway particles in this case, the average velocity $\boldsymbol{u}$ never reaches a quasistationary value and thus keeps on growing. As shown in Fig.5.b, $\boldsymbol{E}$ is oriented in the positive direction of Oz, so that the average velocity u_z of the electrons is negative.

At the end of the run, the distribution has evolved significantly from its initial state, as the temperature increased by a factor two and the distribution has drifted by $u \sim 1.5\, v_{\rm th}$. This clearly illustrates the need for evolving the background in the δf simulation, so that $|\delta f / f|$ remains small. The background $f_{\rm SM}$ at the end of the run, defined by these final values of T and $\boldsymbol{u}$, is plotted in Fig. 5b, together with the component δf and the full distribution $f = f_{\rm SM} + \delta f$ as well as the full distribution obtained by the PIC run. Note that the distribution f obtained by the δf simulation is already significantly less noisy than the distribution given by the PIC run, for the same number $n_p = 10^4$ of particles. This is due to the fact that even in this case of strong drive one has $|\delta f / f| \sim 1/10$, confirming that a Maxwellian was a good choice for the background.

Good agreement between the δf and PIC calculations, as just shown in the particular case of Fig. 5a and 5b, have validated the δf approach with evolving background. In particular, these comparisons also provide an estimate of the error made through the approximations on the self-collision operator. Simulations were then carried out for very weak electric fields, which illustrate the ability of the δf approach to resolve small perturbations.

In Fig. 6a, the average velocity u_z is plotted for $E = 1 \cdot 10^{-4}\, m\overline{\nu}_{ee}(0) v_{\rm th}(0)/e$. The other physical and numerical parameters were kept the same as for the runs with the strong field $[Z = 1, n_p = 10^4, \Delta t = 10^{-2}\, \overline{\nu}_{ee}(0)^{-1}]$. The simulation was carried out over $240\, \overline{\nu}_{ee}(0)^{-1}$. In this linear regime, the system stabilizes to a quasistationary state (even though negligible here, temperature always keeps on increasing due to Ohmic heating), which enables one to evaluate the conductivity $\sigma = e\overline{N}u/E = j/E$. Without the weight spread reduction scheme, one clearly sees in Fig. 6a how noise increases in time, reaching a significant level ($\sim$ 10% of signal) at the end of the run. This is directly related to the evolution of the entropy $S_w = (1/2)\sum w_i^2$, which keeps on increasing linearly in time once the system has reached its quasisteady state, as shown in Fig. 6b. If the run had been prolonged in this way, the signal would ultimately be drowned by the noise. The weight spread reduction procedure, chosen here so as to enforce conservation of density and momentum along $v_\perp$ and v_z, achieves saturation of entropy in the quasisteady state (Fig. 6b), thus providing a signal with no increasing noise (Fig. 6a). In fact, to avoid adding any numerical frequency to the system, which could potentially lead to an artificial instability, the reduction of Δw was carried out at random time intervals, but at an average of every collision time $\overline{\nu}_{ee}(0)^{-1}$. The signal of the PIC simulation, carried out with the same number $n_p = 10^4$ of particles, falls below the noise level in this case. This is illustrated in the inset of Fig. 6, where the PIC and δf results are compared, clearly demonstrating the advantage of the latter method to deal with small deviations from the background.

Figure 7 compares the amplitudes of the components δf and f_{SM} at the end of this low $|\boldsymbol{E}|$ simulation, giving an average ratio $|\delta f/f_{\mathrm{SM}}| \sim 10^{-3}$. Also plotted is the marker particle distribution $g(\boldsymbol{v})$ for both a simulation with and without sources and sinks of markers. Due to the scattering of the particles with the background, g tends to adopt the shape of f_{SM}, as shown in Fig. 7 in the absence of sources and sinks. However, by annihilating the marker particles with a rate $\alpha = 10^{-2}\,\overline{\nu}_{ee}(0)$, and reinjecting the particles uniformly in a shell $v_{\min} < |\boldsymbol{v} - \boldsymbol{u}| < v_{\max}$, with $v_{\min} = 4.25\,v_{\mathrm{th}}$ and $v_{\max} = 4.75\,v_{\mathrm{th}}$, one is able to maintain a much more uniform distribution g up to large velocities. This improved resolution in the tail of f, where electrons have low collisionality and therefore play a major role in determining the current, turned out to improve significantly the results.

Finally, Fig. 8 plots the conductivities computed in the linear regime for different values of the ion ionization Z. The results from the δf approach are compared to the ones by Spitzer and Härm,[18] obtained by solving the Fokker–Planck equation with traditional integration methods, and which are valid to four significant digits. The limit of Z going to infinity, corresponding to the Lorentz conductivity, was obtained by simply neglecting self-collisions between electrons. The difference between the two approaches is less then 10% and provides further validation of the collision model (83)–(85).

C. Second Illustration: Collisional Absorption

Assuming again a homogeneous plasma, the starting equation for studying electron heating through collisional absorption (inverse bremsstrahlung) of laser light is of the same form as Eq.(71), except for the electrical field

$$\boldsymbol{E}(t) = \boldsymbol{E}_0 \cos \omega t,$$

which now oscillates at the frequency ω of the driving laser. However, instead of solving the Fokker–Planck equation on the short time scale of the laser, we will consider here the evolution averaged over the period $\tau_{\text{laser}} = 2\pi/\omega$. Having furthermore assumed that the laser intensity is sufficiently low for the distribution to remain essentially isotropic, Langdon[20] derived the following equation for the slow variation of $f(|\boldsymbol{v}|;t)$:

$$\frac{\partial f}{\partial t} + \mathcal{H} f = -C_{ee}[f,f], \tag{86}$$

$$\mathcal{H} f = -\frac{\overline{\nu}_{ei} v_{\text{th}}^3}{3} \left(\frac{v_0}{v}\right)^2 \frac{\partial}{\partial v}\left[\frac{h(v)}{v}\frac{\partial f}{\partial v}\right], \tag{87}$$

$$h(v) = \frac{1}{1+(v_\omega/v)^6}, \tag{88}$$

where v_ω is defined by $\nu_{ei}(v_\omega) = \omega/2$ and $v_0 = e\,E_0/m\,\omega$ is the amplitude of the velocity oscillation. The combined effect of the oscillating electrical field $\boldsymbol{E}(t)$ and the electron–ion collisions has given rise to the collisional heating term $\mathcal{H}$. Note that this rotationally invariant operator can be written in the drift diffusion form:

$$\mathcal{H} f = \frac{1}{v^2}\left[\frac{\partial}{\partial v}\frac{\langle \Delta v\rangle}{\Delta t}(v^2 f) - \frac{\partial^2}{\partial v^2}\frac{\langle \Delta v^2\rangle}{2\,\Delta t}(v^2 f)\right], \tag{89}$$

$$\frac{\langle \Delta v \rangle}{\Delta t} = \frac{\overline{\nu}_{ei} {v_{\rm th}}^3}{3} \left(\frac{v_0}{v}\right)^2 \frac{d}{dv}\left[\frac{h(v)}{v}\right], \tag{90}$$

$$\frac{\langle (\Delta v)^2 \rangle}{2\Delta t} = \frac{\overline{\nu}_{ei} {v_{\rm th}}^3}{3} \left(\frac{v_0}{v}\right)^2 \frac{h(v)}{v}, \tag{91}$$

and for numerical implementation can therefore be dealt with in the same way as the collision operators.

Equation (86) was solved by applying the δf approach described in Sec. III A, again considering decomposition (50) and constraints (52). As (86) now takes a somewhat different form than (71), one cannot make direct use of the set of fluid and marker particle equations (72)–(74) and (75)–(77). However, it is straightforward to derive a corresponding system. Redefining the operator

$$\frac{D}{Dt} = \frac{\partial}{\partial t} + \mathcal{H} + C_{ei}[f_{\rm M},\ ], \tag{92}$$

the equation for $\delta f(|\boldsymbol{v}|;t)$ can still be written in the form (55), after having again approximated the self-collision operator $C_{ee}[f,f]$ by $\widehat{C}\delta f$. Taking the first three velocity moments of the equation for δf leads to the following set of fluid equations for the background parameters $[N(t), \boldsymbol{u}(t), v_{\rm th}(t)]$:

$$\frac{dN}{dt} = 0, \quad \Longrightarrow \quad N(t) = \overline{N} = \text{const.}, \tag{93}$$

$$m\overline{N}\frac{d\boldsymbol{u}}{dt} = 0 \quad \Longrightarrow \quad \boldsymbol{u}(t) = \boldsymbol{u}(t=0) = 0, \tag{94}$$

$$\frac{d}{dt}(\frac{3}{2}\overline{N}\,T) = Q_{ca}(f_{\rm M}) + Q_{ca}(\delta f), \tag{95}$$

with $Q_{ca}(f) = Q_{ca}(f_{\rm M}) + Q_{ca}(\delta f)$ standing for the heat generated in f by collisional absorption:

$$Q_{ca}(f) = -\frac{m\overline{N}}{2}\int d\boldsymbol{v}\, v^2 \mathcal{H} f.$$

The contributions from $f_{\rm M}$ and δf can be given more explicitly in the form:

$$Q_{ca}(f_{\rm M}) = \overline{\nu}_{ei} m\overline{N} v_0^2\, I[(v_\omega/2v_{\rm th})^2],$$

$$Q_{ca}(\delta f) = \frac{m\overline{N}}{2}\sum_{i=1}^{n_p} w_i \frac{d}{dt_{ca}}({\boldsymbol{v}_i}^2),$$

where d/dt_{ca} stands for the variation due to collisional absorption scattering defined by (90)–(91). The integral $I(x)$ can be expressed in terms of the complex exponential integral $E_1(z)$:[21]

$$\begin{aligned}\frac{3\sqrt{2\pi}}{2} I(x) &= \int_0^{+\infty} d\epsilon \frac{\epsilon^3\, e^{-\epsilon}}{\epsilon^3 + x^3} \\ &= 1 - \frac{x}{3}\left\{ e^x E_1(x) - 2\, e^{-x/2}\,\mathrm{Re}\left[\exp i(\frac{\pi}{3} - x\frac{\sqrt{3}}{2})\, E_1(-x\, e^{i\pi/3})\right]\right\}.\end{aligned}$$

Note that the background is now simply denoted f_M, instead of f_SM as the shift $\boldsymbol{u}$ is zero.

Having again chosen equation (61) for the marker particle distribution $g(|\boldsymbol{v}|;t)$, with D/Dt now given by (92), one can derive the following equations for the particle trajectories in the extended phase space:

$$\frac{d\boldsymbol{v}}{dt} = \boldsymbol{a}_{ca} + \boldsymbol{a}_{ei}, \tag{96}$$

$$\frac{dw}{dt} = -\frac{p}{f_\mathrm{M}}\left(\frac{D}{Dt} f_\mathrm{M} + f_\mathrm{M}\mathcal{O}\delta f\right), \tag{97}$$

$$\frac{dp(t)}{dt} = \frac{p}{f_\mathrm{M}}\frac{D}{Dt} f_\mathrm{M}, \tag{98}$$

with the approximation $C_{ee}[\delta f, f_\mathrm{M}] \simeq f_\mathrm{M}\mathcal{O}\delta f$ given by (47). Note that for this problem we have not added any sources and sinks of markers, as high resolution in the tail of the distribution is not as critical as for computing Spitzer conductivity. In (96), $\boldsymbol{a}_{ca}$ and $\boldsymbol{a}_{ei}$ stand for the random accelerations related to collisional absorption and electron–ion scattering respectively. Finally, the term D/Dt appearing in (97) and (98) can be written explicitly:

$$\frac{1}{f_\mathrm{M}}\frac{D}{Dt} f_\mathrm{M} = \frac{d\ln T}{dt}\left(\frac{v^2}{2{v_\mathrm{th}}^2} - \frac{3}{2}\right) + \frac{\overline{\nu}_{ei}}{3}\left(\frac{v_0}{v}\right)^2\left(v_\mathrm{th}\frac{dh(v)}{dv} - h(v)\frac{v}{v_\mathrm{th}}\right).$$

1. Results for Collisional Absorption

As when computing electrical Spitzer conductivity, the simulations were initialized with a Maxwellian distribution, so that $\delta f(t=0) = 0$. The shape the distribution adopts in the following evolution depends on the relative importance between the two competing effects: Self collisions between electrons, tending to maintain a Maxwellian, and collisional absorption, which deforms f into a more flat-topped distribution. The relevant parameter here is thus given by

$$\gamma = Z\left(\frac{v_0}{v_{\rm th}}\right)^2 \sim \mathcal{H}/C_{ee},$$

which estimates in (86) the relative importance of the collisional absorption operator $\mathcal{H}$ with respect to the collision operator C_{ee}. The assumption of low laser intensity for deriving Eq.(86) implies $v_0/v_{\rm th} \ll 1$. By considering a high Z plasma, the parameter γ can nonetheless take large values.

For a first run, we assumed $v_0 = 0.2\, v_{\rm th}(0)$ and $Z = 10$, giving an initial value $\gamma(0) = 0.4$. Furthermore, the laser frequency ω was fixed such that $v_\omega = 0.35\, v_{\rm th}(0)$. The number of marker particles was chosen $n_p = 10^4$. Naturally, γ varies in time as the electron distribution heats up and the thermal velocity $v_{\rm th}$ of the background increases. After $t = 40\, \overline{\nu}_{ee}(0)^{-1}$, the parameter thus was reduced to $\gamma \simeq 0.3$, and the distribution adopted the shape given by the dashed line in Fig. 9a.

The simulation was then repeated without considering self-collisions, which corresponds to the limit $\gamma \to \infty$. After the same run time, f had evolved towards the distribution given by the full line in Fig. 9a, which approaches the self-similar solution $f \sim \exp(-v^5/5\, u^5)$.[20] In this case, the deviation δf of f from the Maxwellian background $f_{\rm SM}$, which is also plotted in Fig. 9a, becomes relatively important, so that the δf approach lost most of its advantage over a PIC calculation.

The evolution of the background temperature T in time is given in Fig. 9b. The fluid calculation, obtained by solving (95) after having discarded the closure term $Q_{ca}(\delta f)$, is also indicated. As discussed in Ref. 20, the heating rate dT/dt is directly proportional to the fraction of particles at low velocities. This can be verified in Fig. 9. Indeed, first note that all three curves $T(t)$ start with the same slope at $t = 0$, due to the fact that the runs were all initialized with the same Maxwellian. Second, the final states at $t = 40\, \overline{\nu}_{ee}(0)^{-1}$ correspond respectively to the three distributions appearing in Fig. 9a, and one can easily check that the different slopes dT/dt are proportional to the different values of $f(v = 0)$.

IV. CONCLUSIONS

The possibility of extending the δf approach for simulating the evolution of a collisional plasma over transport time scales has been investigated. This resulted in a hybrid fluid–kinetic procedure. Numerically "cheap" fluid equations are solved for advancing a Maxwellian background f_{SM}, which is supposed to provide at all times a good approximation of the full distribution f. Relatively few weighted marker particles are then required for representing the remainder δf. Potentially, the advantages of such a particle approach over a "standard" integration scheme using finite differences or finite elements is at least threefold: (1.) Thanks to its Monte-Carlo-type sampling, a particle code requires less points for representing a distribution in high dimensionality. (2.) Particles can easily be evolved such that they remain in the active regions of phase space, while a good fraction of a fixed mesh grid usually remains idle during most of the simulation. (3.) Particle codes are well suited for making use of today's massively parallel computers, contrary to implicit time algorithms applied for evolving a distribution over a grid.

At present, proof of principal has been given through two test cases involving the evolution of an homogeneous electron distribution colliding with themselves and with cold ions. The system was first driven by a constant electric field, then, in the second illustration, it was heated through collisional absorption. These two test cases should provide a useful starting point for attempting to apply these methods to an inhomogeneous plasma, with the intention of studying the nonclassical drive and transport in laser–plasma interaction.[22–25]

Independently of the problem of evolving the background, much emphasis was put in this paper on how to deal with the issue of increasing numerical noise due to the spreading of marker weights in a collisional δf simulation. Let us again point out that this effect is independent of the approximations on the self-collision operator $C[f, f]$ which were taken here, i.e., linearization of the Landau operator $C[f, f]$, and simplification of $C_{ee}[\delta f, f_{\mathrm{SM}}]$. Hence, weight spreading will be generated by any type of collisions throughout the simulation. Although we have not been able to derive a useful general estimate, the results obtained here should provide a reference: Spreading proportional to the square root of time, and noise/signal ratio near 10% after approximately one hundred collisional times when using a reasonable number of 10^4 particles for representing velocity space. A procedure for limiting this spreading has been proposed, and basically consists of "cooling" the weights of markers as they randomly enter the more densely populated regions of phase space. This needs only to be carried out periodically in time and only within a limited number of bins in phase space. In each of these cells a regression over the weights is computed, and their values are reassigned to this average fit. Depending on the order of the regression, the scheme ensures conservation of different physical averages such as number of particles, momentum, and kinetic energy. In the future, we shall also look into alternative ways of dealing with the weight spreading, such as applying thermostats, initially devised for dissipating the ever finer structures which develop in phase space in otherwise collisionless systems.[16] Conversely, the regressions employed in the weight spread reduction scheme might serve as an alternative way of removing those fine structures in collisionless simulations.

ACKNOWLEDGMENTS

This work was supported by the Lawrence Livermore National Laboratory under DOE Interoffice Work Order Number B344523, by the U.S. Department of Energy Contract No. DE–AC02–76–CHO–3073, and by the Swiss National Science Foundation.

APPENDIX A: PROPERTIES OF THE APPROXIMATION $\widehat{C} \simeq C[f_{\rm M}, \delta f] + f_{\rm M}\mathcal{O}\delta f$ FOR THE LINEARIZED COLLISION OPERATOR.

A straightforward calculation enables one to show that $\widehat{C} = C[f_{\rm M}, \delta f] + C[\delta f, f_{\rm M}]$, approximated with $C[f_{\rm M}, \delta f] \simeq f_{\rm M}\mathcal{O}\delta f$, still conserves the collision invariants (particle number, momentum, kinetic energy). Let us prove here that the approximated $\widehat{C}$ also still annihilates functions of the form (4). In fact, it is sufficient to show that $\widehat{C}$ remains self-adjoint with respect to the scalar product $\langle a|b\rangle$, where:

$$\langle a| = \int d\boldsymbol{v}\, a(\boldsymbol{v}),$$
$$|b\rangle = f_{\rm M}(\boldsymbol{v})\, b(\boldsymbol{v}).$$

Indeed, the conservation of particle number, momentum, and kinetic energy can then be written

$$\langle \boldsymbol{v}^{\,j}|\widehat{C} = 0, \quad j = 0, 1, 2,$$

which in conjugate form leads to the end of the proof:

$$\widehat{C}^{\dagger}|\boldsymbol{v}^{\,j}\rangle = \widehat{C}\,\boldsymbol{v}^{\,j} f_{\rm M}(v) = 0, \quad j = 0, 1, 2.$$

One can actually demonstrate that $C[f_{\rm M}, \delta f]$ and $f_{\rm M}\mathcal{O}\delta f$ are self-adjoint independently:

- Upon inserting (2), one shows that $C[f_{\rm M}, \delta f]$ is self-adjoint:

$$\begin{aligned}
\langle a|C[f_{\rm M},\ ]|b\rangle &= \Gamma \int d\boldsymbol{v}\, a(\boldsymbol{v}) \frac{\partial}{\partial \boldsymbol{v}}\boldsymbol{\cdot} \int d\boldsymbol{v}\,'\, \mathsf{U}\boldsymbol{\cdot} \left(\frac{\partial}{\partial \boldsymbol{v}\,'} - \frac{\partial}{\partial \boldsymbol{v}}\right) f_{\rm M}(v')\, f_{\rm M}(v) b(\boldsymbol{v}) \\
&= -\Gamma \int d\boldsymbol{v}\, d\boldsymbol{v}\,'\, f_{\rm M}(v)\, f_{\rm M}(v')\, \frac{\partial a(\boldsymbol{v})}{\partial \boldsymbol{v}}\boldsymbol{\cdot}\mathsf{U}\boldsymbol{\cdot}\frac{\partial b(\boldsymbol{v})}{\partial \boldsymbol{v}} \\
&= \langle b|C[f_{\rm M},\ ]|a\rangle,
\end{aligned}$$

  having integrated by parts, used the fact that U is symmetric and $\mathsf{U}\boldsymbol{\cdot}(\boldsymbol{v} - \boldsymbol{v}\,') = 0$.

- Making use of

$$\int C[f_{\rm M},\delta f]\,\boldsymbol{v}\,d\boldsymbol{v} = \overline{\nu} v_{\rm th}\int H\frac{\boldsymbol{v}}{v_{\rm th}}\,\delta f(\boldsymbol{v})\,d\boldsymbol{v}, \tag{A1}$$

$$\int C[f_{\rm M},\delta f]\,v^2\,d\boldsymbol{v} = \overline{\nu} v_{\rm th}^2\int \left[2(v/v_{\rm th})^2\,H\,-\,H\,-\,K\right]\delta f(\boldsymbol{v})\,d\boldsymbol{v}, \tag{A2}$$

together with relations (48)–(49), enables one to show that $f_{\rm M}\mathcal{O}\delta f$ is self-adjoint:

$$\begin{aligned}
\langle a|f_{\rm M}\mathcal{O}|b\rangle &= \int d\boldsymbol{v}\,a(\boldsymbol{v})f_{\rm M}(v)\left\{\frac{6\sqrt{\pi}}{v_{\rm th}}\,\boldsymbol{\mathcal{P}}(f_{\rm M}\,b)\boldsymbol{\cdot}\,H\,\frac{\boldsymbol{v}}{v_{\rm th}} + \frac{\sqrt{\pi}}{v_{\rm th}^2}\,\mathcal{E}(f_{\rm M}b)\left[2(v/v_{\rm th})^2\,H - H - K\right]\right\} \\
&= -\frac{6\sqrt{\pi}}{\overline{\nu} v_{\rm th}^2}\int C[f_{\rm M},f_{\rm M}\,a]\,\boldsymbol{v}\,d\boldsymbol{v}\boldsymbol{\cdot}\int C[f_{\rm M},f_{\rm M}\,b]\,\boldsymbol{v}\,d\boldsymbol{v} \\
&\quad -\frac{\sqrt{\pi}}{\overline{\nu} v_{\rm th}^4}\int C[f_{\rm M},f_{\rm M}\,a]\,v^2\,d\boldsymbol{v}\int C[f_{\rm M},f_{\rm M}\,b]\,v^2\,d\boldsymbol{v} \\
&= \langle b|f_{\rm M}\mathcal{O}|a\rangle.
\end{aligned}$$

This last derivation can be used directly for reevaluating equation (37) for the approximation $C[\delta f, f_{\rm M}] \simeq f_{\rm M}\mathcal{O}\delta f$:

$$\begin{aligned}
\frac{d}{dt}\mathcal{S}_w(t) &= -\frac{1}{n_p}\int\frac{\delta f}{f_{\rm M}}C[\delta f,f_{\rm M}]\,d\boldsymbol{v} \\
&\simeq -\frac{1}{n_p}\int\delta f\,\mathcal{O}\delta f\,d\boldsymbol{v} = -\frac{1}{n_p}\langle\delta f/f_{\rm M}\,|\,f_{\rm M}\mathcal{O}\,|\,\delta f/f_{\rm M}\rangle \\
&= \frac{\sqrt{\pi}}{n_p\overline{\nu}}\left[\frac{6}{v_{\rm th}^2}\left(\int C[f_{\rm M},\delta f]\,\boldsymbol{v}\,d\boldsymbol{v}\right)^2 + \frac{1}{v_{\rm th}^4}\left(\int C[f_{\rm M},\delta f]\,v^2\,d\boldsymbol{v}\right)^2\right],
\end{aligned} \tag{A3}$$

which is manifestly positive for all δf. With the help of Eqs. (A1)–(A2), one can then easily evaluate (A3) for δf having reached a stationary state of the form (4):

$$\frac{d}{dt}\mathcal{S}_w(t) = \frac{\overline{\nu}}{\sqrt{\pi}n_p}\left(\frac{c_1^2}{6}+c_2^2\right), \tag{A4}$$

corresponding to the modification of (38).

APPENDIX B: A PRACTICAL APPROACH FOR IMPLEMENTING SOURCES AND SINKS OF MARKER PARTICLES.

In some situations, one may want to take advantage of the possibility, pointed out in reference,[11] of adding sources and sinks of marker particles to the δf simulation. As these sources and sinks are independent of the physical system being represented, one is free to define them so as to be convenient for numerical implementation, and so as to ensure a high density of markers in regions of phase space where δf requires high resolution.

As a practical approach, sinks are defined by assigning each particle the same probability $p_\dagger = \exp(-\alpha\Delta t)$ of being annihilated at each time step Δt. The lifetime of the marker particles is thus given by a random exponential distribution with annihilation rate α. To conserve the total number of particles, sources are defined so that annihilated markers are immediately reinjected into the extended phase space according to a convenient random distribution $S(\boldsymbol{x}, \boldsymbol{v}, w, p)$.

Let us note $dw/dt = \dot{w}$ and $dp/dt = \dot{p}$, the weight equations in the absence of sources. These must now be completed with correction terms to account for the death and birth of neighboring marker particles:

$$\dot{w}_+ \doteq \frac{dw}{dt} = \dot{w} + \alpha\, w - \frac{p}{f_{\mathrm{SM}}} \int S(\boldsymbol{x}, \boldsymbol{v}, w, p)\, w\, dw\, dp, \tag{B1}$$

$$\dot{p}_+ \doteq \frac{dp}{dt} = \dot{p} + \alpha\, p - \frac{p}{f_{\mathrm{SM}}} \int S(\boldsymbol{x}, \boldsymbol{v}, w, p)\, p\, dw\, dp. \tag{B2}$$

One can prove that these new equations still represent the same fields δf and f_{SM}, while correctly taking into account the effects of sources and sinks. This is carried out by writing the Fokker–Planck equation for the distribution $F(\boldsymbol{x}, \boldsymbol{v}, w, p; t)$ in the extended phase space, first without the sources and sinks:

$$\frac{D}{Dt} F + \frac{\partial}{\partial w}(\dot{w} F) + \frac{\partial}{\partial p}(\dot{p} F) = 0, \tag{B3}$$

and then with

$$\frac{D}{Dt} F + \frac{\partial}{\partial w}(\dot{w}_+ F) + \frac{\partial}{\partial p}(\dot{p}_+ F) = -\alpha F + S(\boldsymbol{x}, \boldsymbol{v}, w, p). \tag{B4}$$

The operator D/Dt determines the evolution in the physical space $(\boldsymbol{x}, \boldsymbol{v})$, as given for instance by (56). One can then easily show that by taking the moments $\int w \, dw \, dp$ and $\int p \, dw \, dp$ of both (B3) and (B4), and identifying (70)–(69), one indeed recovers the same equations for the physical fields δf and $f_{\rm SM}$. Naturally, by taking the moment $\int dw \, dp$ of (B4), one obtains an equation for the marker particle distribution $g(\boldsymbol{x}, \boldsymbol{v}; t)$ in the physical space, which reflects the existence of sources and sinks:

$$\frac{D\,g}{Dt} = -\alpha g + \int S \, dw \, dp.$$

By further taking the moment $\int d\boldsymbol{x} \, d\boldsymbol{v}$ of this last relation, one obtains the condition on S for conservation of the total number n_p of markers:

$$\int S(\boldsymbol{x}, \boldsymbol{v}, w, p) \, d\boldsymbol{x} \, d\boldsymbol{v} \, dw \, dp = \alpha \, n_p.$$

In fact, when a simulation including sources and sinks as described above is carried out together with the weight spread reduction scheme of Sec. II G, equations (B1)–(B2) can take an even simpler form. This is achieved by choosing

$$S(\boldsymbol{x}, \boldsymbol{v}, w, p) = s(\boldsymbol{x}, \boldsymbol{v}) \, \delta(w) \, \delta(p),$$

that is, reinjecting markers with zero weights. This choice removes the last terms in (B1) and (B2). In general, the equation of motions for the weights are linear and homogeneous with respect to w and p. As an effect, the weights of newborn particles would remain zero and these markers would therefore seem to be wasted. However, thanks to the weight reduction scheme, initially weightless particles are rapidly reassigned new nonzero values for (w, p), and weights of neighboring particles are corrected to account for the presence of these new markers.

Let us still point out that for the above discussion the background need not be a Maxwellian and that the notation $f_{\rm SM}$ was kept for convenience.

REFERENCES

[1] M. Kotschenreuther, Bull. Am. Phys. Soc. **34** 2107 (1988).

[2] M. Kotschenreuther, in *Proceedings of the 14th International Conference on the Numerical Simulation of Plasmas* (Office of Naval Research, Arlington, VA, 1991), Paper PT20.

[3] S. E. Parker and W. W. Lee, Phys. Fluids B **5**, 77 (1993).

[4] Z. Lin, T. S. Hahm, W. W. Lee, W. M. Tang, and R. B. White, Science **281**, 1835 (1998).

[5] A. Y. Aydemir, Phys. Plasmas **1**, 822 (1994).

[6] G. Hu and J.A. Krommes, Phys. Plasmas **1**, 863 (1994).

[7] D. C. Barnes, *14 th International Conference on the Numerical Simulation of Plasmas*, (Annapolis, Md, 1991), Paper PWE6.

[8] X. Q. Xu and M. N. Rosenbluth, Phys. Fluids B **3**, 627 (1991).

[9] A. M. Dimits and B. I. Cohen, Phys. Rev. E **49**, 709 (1994).

[10] Z. Lin, W. M. Tang, and W. W. Lee, Phys. Plasmas **2**, 2975 (1995).

[11] Y. Chen and R. B. White, Phys. Plasmas **4**, 3591 (1997).

[12] T. D. Rognlien and T. A. Cutler, Nucl. Fusion **20**, 1003 (1980).

[13] M. N. Rosenbluth, W. M. MacDonald, and D. L. Judd, Phys. Rev. **107**, 1 (1957).

[14] W. W. Lee and W. Tang, Phys. Fluids **31**, 612 (1988).

[15] J. A. Krommes and Genze Hu, Phys. Plasmas **1**, 3211 (1994).

[16] J. A. Krommes, *Thermostatted* δf, Phys. Plasmas, in press.

[17] S. I. Braginskii, in *Reviews of Plasma Physics* (Consultants Bureau, New York, 1965), Vol. 1.

[18] L. Spitzer, Jr. and R. Härm, Phys. Rev. **89**, 977 (1953).

[19] T. Takizuka and H. Abe, Jour. Comp. Phys. **25**, 205 (1977).

[20] A. B. Langdon, Phys. Rev. Lett. **44**, 575 (1980).

[21] I. S. Gradshteyn and I. M. Ryzhik, *Table of Integrals, Series, and Products* (Academic, New York, 1965).

[22] J. P. Matte and J. Virmont, Phys. Rev. Lett., **49**, 1936 (1982).

[23] J. R. Albritton, Phys. Rev. Lett. **50**, 2078 (1983).

[24] E. M. Epperlein, R. W. Short, and A. Simon, Phys. Rev. Lett. **69**, 1765 (1992).

[25] A. V. Brantov, V. Yu. Bychenkov, V. T. Tikhonchuk, and W. Rozmus, Phys. Plasmas **5**, 2742 (1998).

FIGURE CAPTIONS

Fig.1 Schematic representation of marker particle weights in phase space for a collisionless (a) and collisional (b) simulation. In the collisional case, the nonzero local spread Δw appears like a growing additional dimension to the numerical system.

Fig.2 Exact (dashed dotted line) and computed (full) weight field $W(v_\perp = 1.2\, v_{\mathrm{th}}, v_z; t)$ after running the simulation one hundred collision times (a) without, and (b) with the weight spread reduction procedure. Estimates of the spreading Δw are given by the dashed lines. The dotted vertical lines indicate the boundaries of the velocity bins.

Fig.3 Evolution in time of (a) entropy $\mathcal{S}_w$ and (b) total deviation of δf from the exact solution $\delta f_{\mathrm{exact}}$ for simulations without (dashed line) and with (full) the reduction procedure.

Fig.4 Evolution in time of total momentum in δf along Oz having applied different orders of regression for reconstructing W in the weight spread reduction scheme.

Fig.5 Results obtained for $|\boldsymbol{E}|$ of the order of the thermal runaway field. Figure 5a gives temperature T and average velocity u_z along $\boldsymbol{E}$, as a function of time t. Shown are results from the δf approach with evolving background (full line), the PIC simulation (dash-dotted), and the fluid calculation (dash-dotted). The projection onto $Oz \| \boldsymbol{E}$ of the distributions in their state at the end of the run appear in Fig. 5b. Given are the background f_{SM} (full line), δf (labeled with $\diamond$), full distribution from the δf approach ($\circ$), and the full distribution from PIC ($\star$).

Fig.6 Results obtained for $|\boldsymbol{E}|$ in the range of the linear regime, enabling one to compute electrical Spitzer conductivity. Figure 6a plots the average velocity u_z as a function of time t. Without applying the weight spread reduction scheme (full line), there is increasing noise on the signal. Thanks to this procedure (dashed line), the statistical fluctuation level remains constant. The inset compares the δf and PIC results for the same number of particles $n_p = 10^4$. Figure 6b shows the evolution of entropy S_w for both runs with and without the Δw reduction scheme.

Fig.7 Projections onto $Oz \| \boldsymbol{E}$ of distributions at the end of the run with low electrical field $|\boldsymbol{E}|$. Plotted are the background f_{SM} (dashed line), δf (labeled with $\diamond$), as well as the marker particle distribution g with ($\circ$) and without ($\star$) sources and sinks.

Fig.8 Electrical Spitzer conductivity for different ionization degrees Z of the ions. Results obtained with the δf approach ($\bigtriangledown$) are compared with the results of Spitzer and Härm ($\circ$).

Fig.9 (a.) Shapes of electron distribution for increasing values of the parameter $\gamma = Z(v_0/v_{\mathrm{th}})$, corresponding to increasing importance of collisional absorption over the relaxation through self collisions. (b.) Increase of temperature due to collisional absorption. Shown are results with (dashed line) and without (full) e–e collisions, as well as the fluid calculation (dash-dotted). The final states correspond respectively to the three distributions plotted in (a.).

FIG.1 Brunner

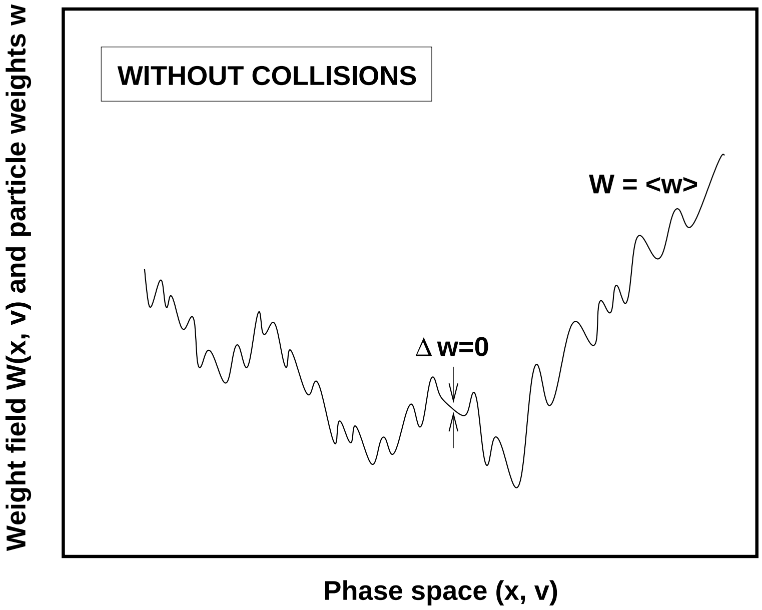

a.)

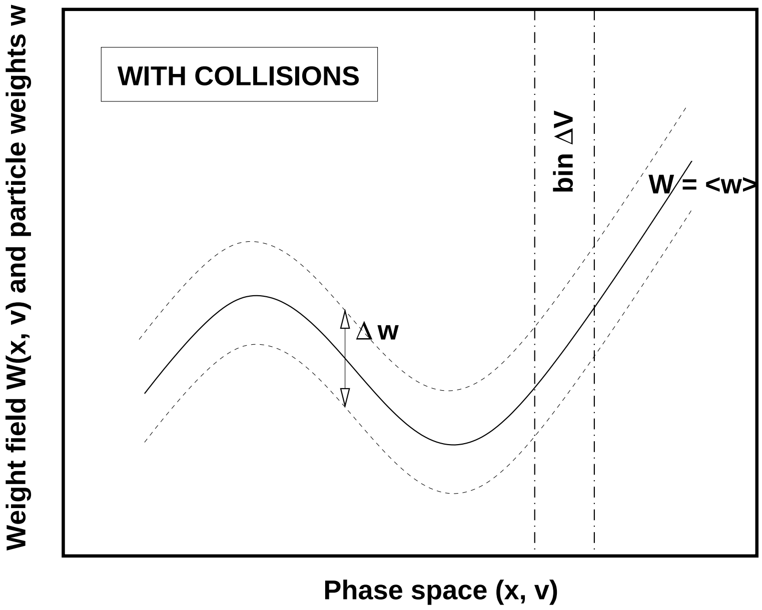

b.)

FIG.2 Brunner

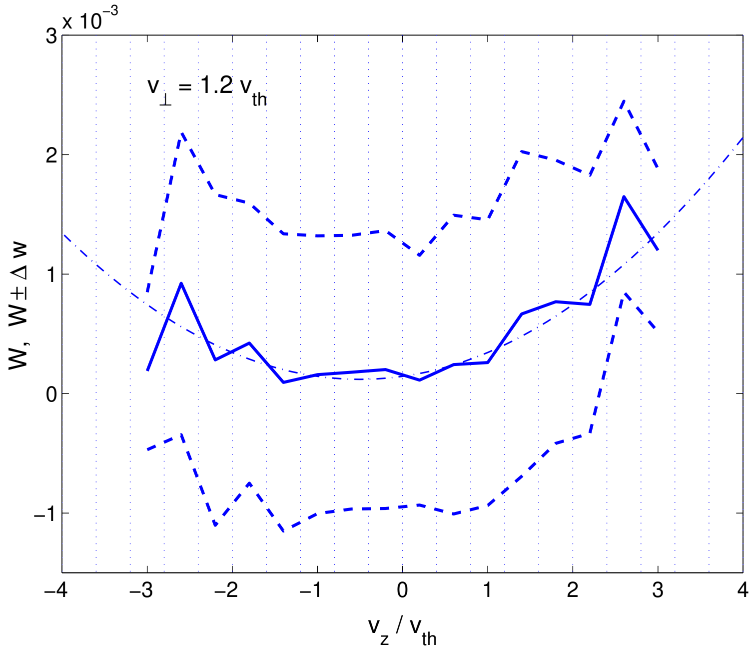

a.)

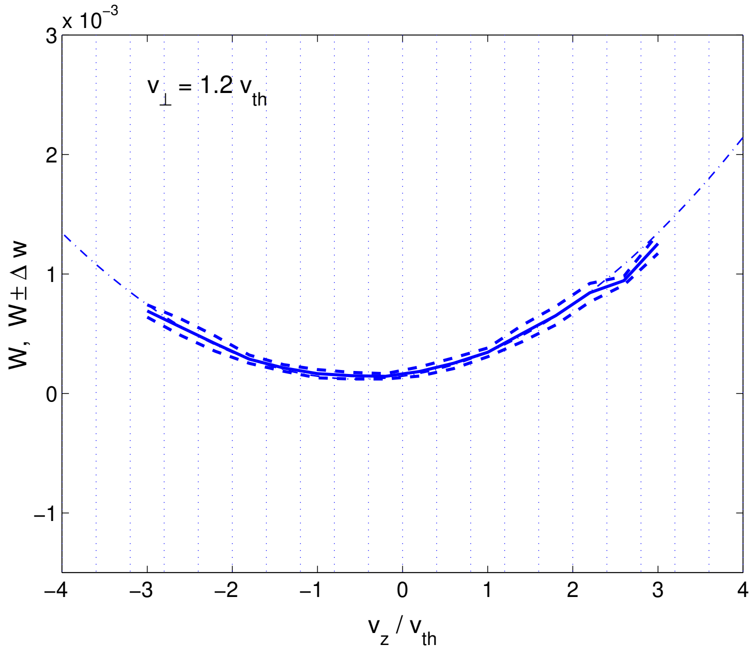

b.)

FIG.3 Brunner

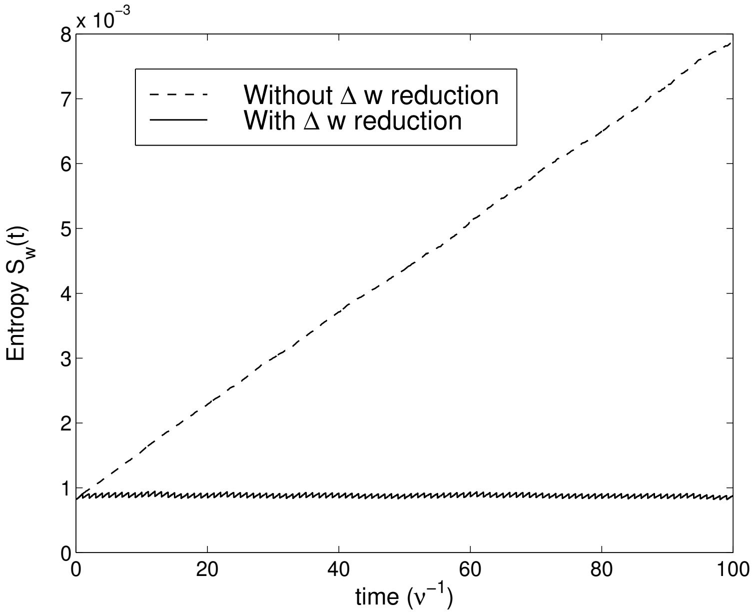

a.)

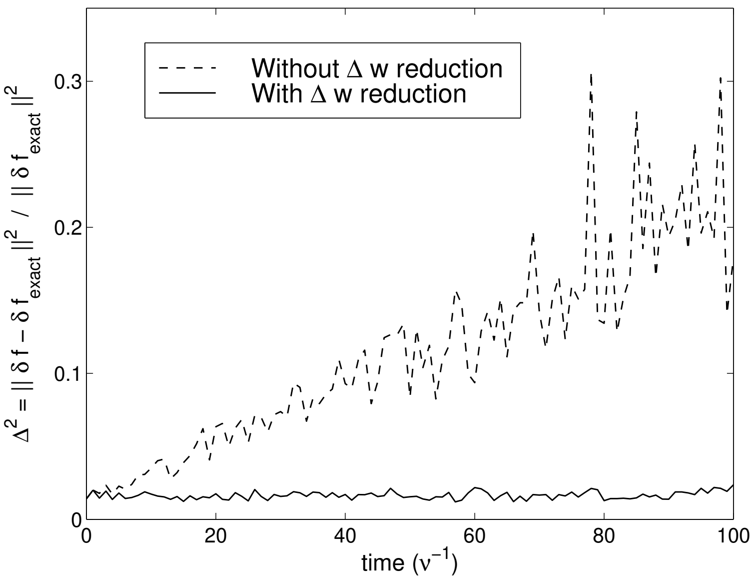

b.)

FIG.4 Brunner

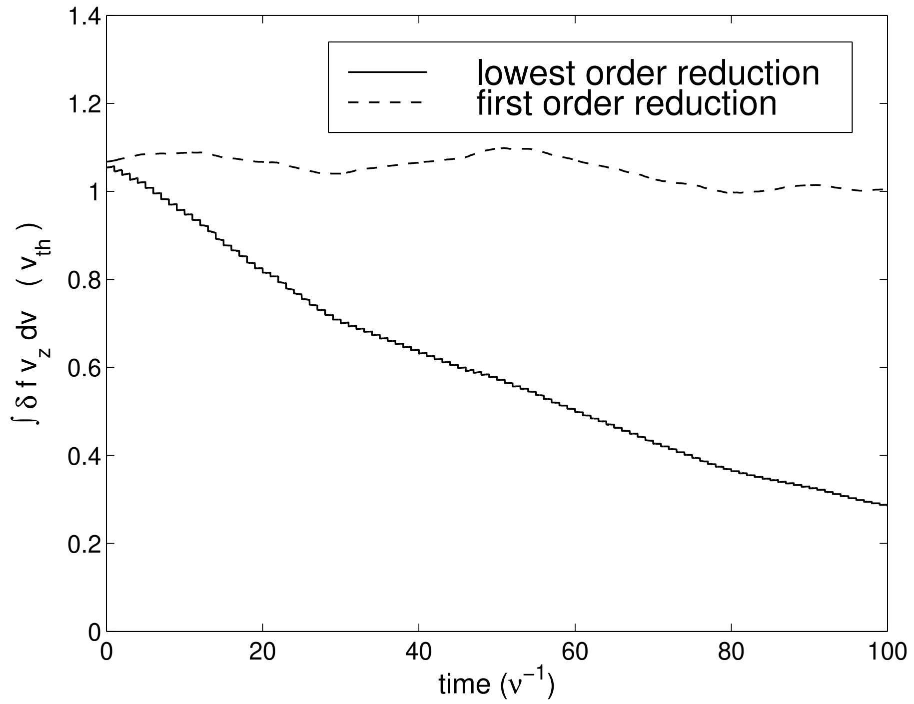

FIG.5 Brunner

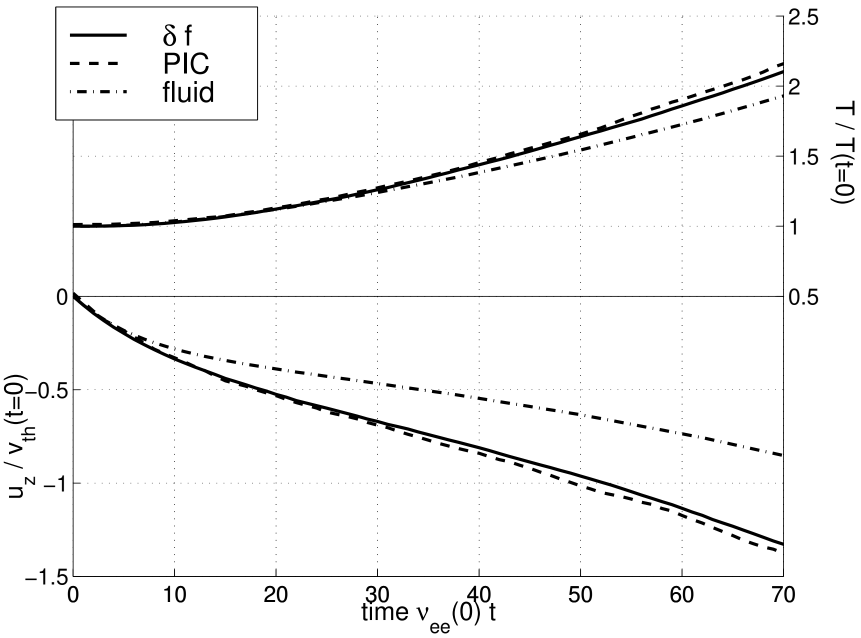

a.)

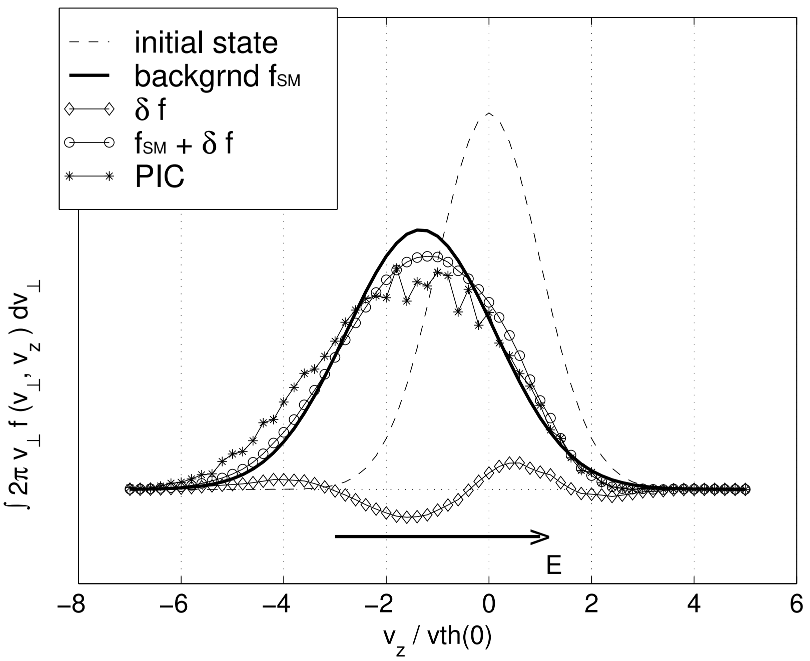

b.)

FIG.6 Brunner

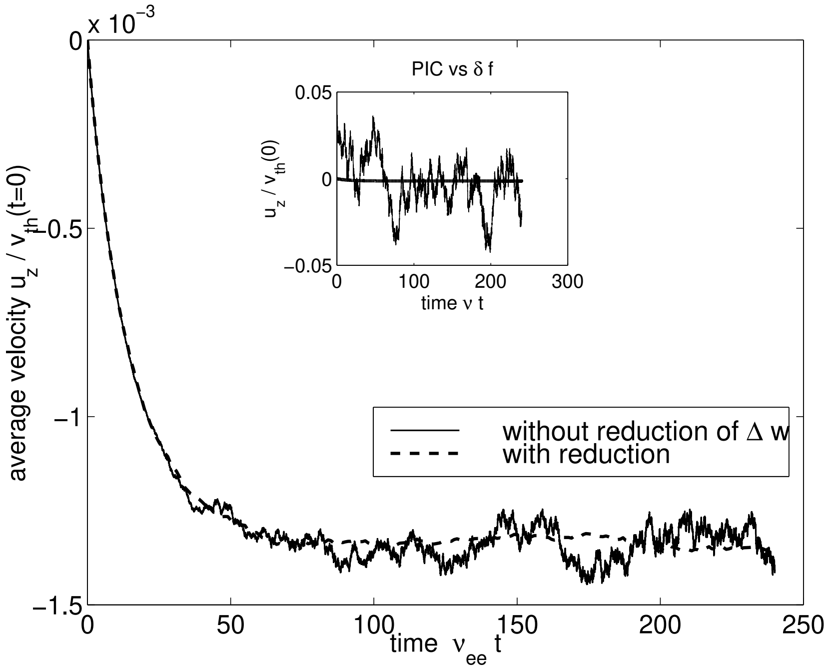

a.)

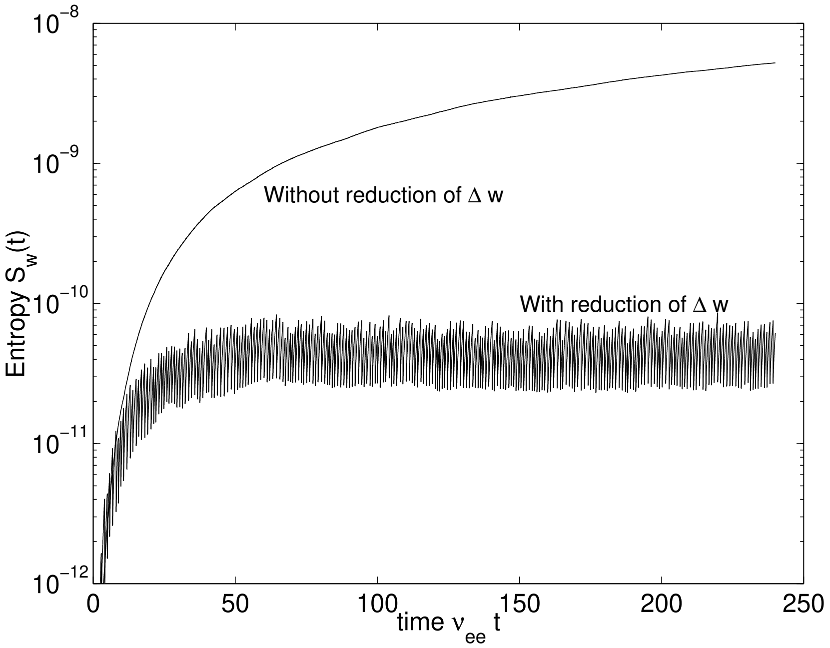

b.)

FIG.7 Brunner

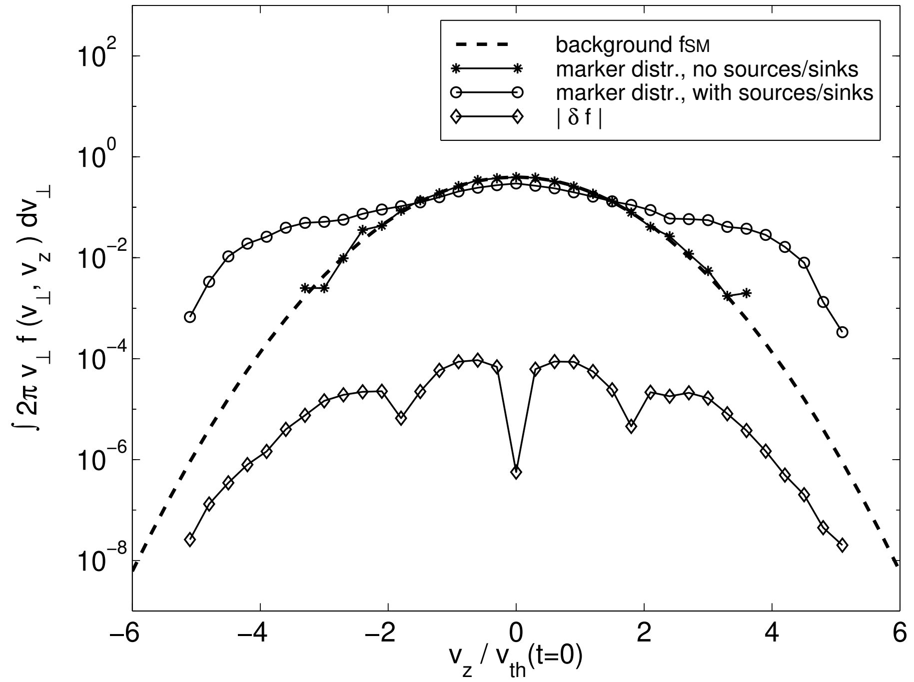

FIG.8 Brunner

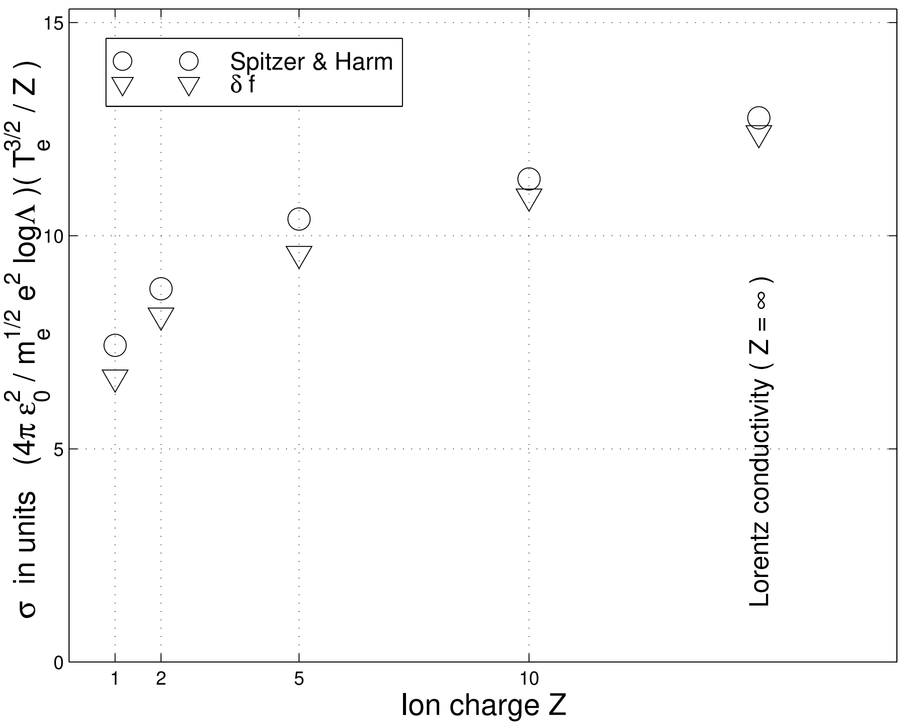

FIG.9 Brunner

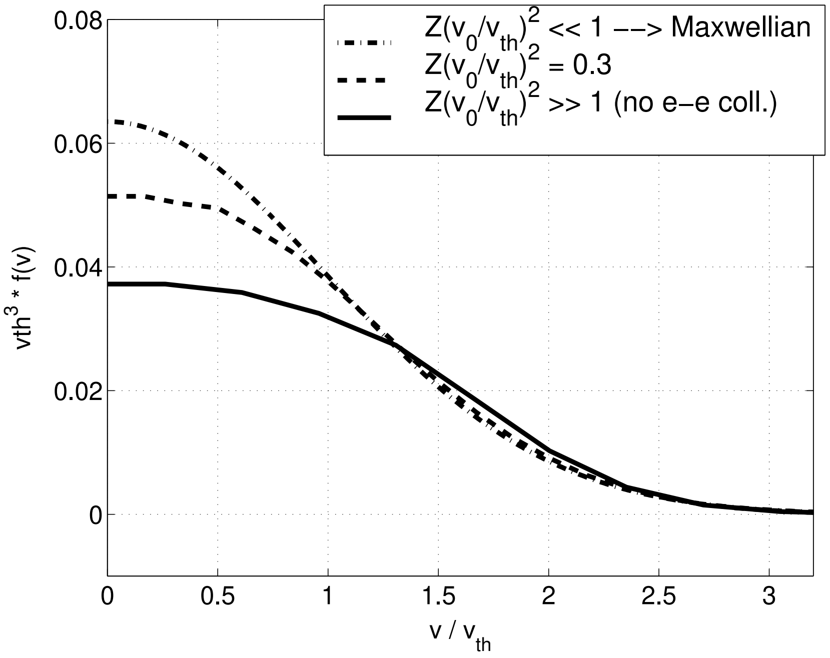

a.)

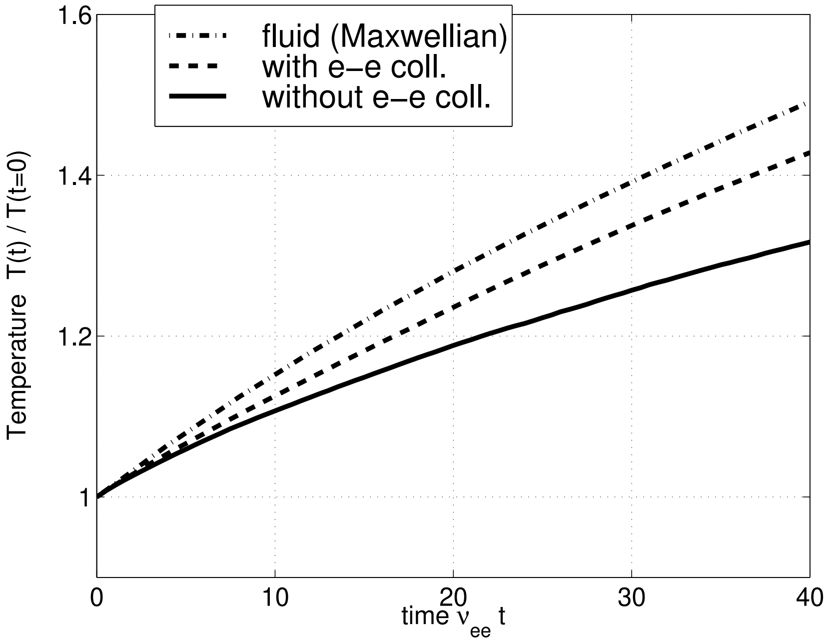

b.)